

FIRST RESULTS FROM A PHOTOMETRIC SURVEY OF STRONG GRAVITATIONAL LENS ENVIRONMENTS

KURTIS A. WILLIAMS AND IVELINA MOMCHEVA
Steward Observatory
933 N. Cherry Ave., Tucson, AZ 85721

CHARLES R. KEETON
Department of Physics and Astronomy
Rutgers University
136 Frelinghuysen Rd., Piscataway, NJ 08854

ANN I. ZABLUDOFF
Steward Obs.
933 N. Cherry Ave., Tucson, AZ 85721

AND

JOSEPH LEHÁR¹
Harvard-Smithsonian Center for Astrophysics
60 Garden Street
Cambridge, MA 02138

Accepted for publication in the Astrophysical Journal

ABSTRACT

Many strong gravitational lenses lie in complex environments, such as poor groups of galaxies, that significantly bias conclusions from lens analyses. We are undertaking a photometric survey of all known galaxy-mass strong lenses to characterize their environments and include them in careful lens modeling, and to build a large, uniform sample of galaxy groups at intermediate redshifts for evolutionary studies. In this paper we present wide-field photometry of the environments of twelve lens systems with $0.24 \leq z_{\text{lens}} \leq 0.5$. Using a red-sequence identifying technique, we find that eight of the twelve lenses lie in groups, and that ten group-like structures are projected along the line of sight towards seven of these lenses. Follow-up spectroscopy of a subset of these fields confirms these results. For lenses in groups, the group centroid position is consistent with the direction of the external tidal shear required by lens models. Lens galaxies are not all super- L_* ellipticals; the median lens luminosity is $\lesssim L_*$, and the distribution of lens luminosities extends 3 magnitudes below L_* (in agreement with theoretical models). Only two of the lenses in groups are the brightest group galaxy, in qualitative agreement with theoretical predictions. As in the local Universe, the highest velocity-dispersion (σ) groups contain a brightest member spatially coincident with the group centroid, whereas lower- σ groups tend to have an offset brightest group galaxy. This suggests that higher- σ groups are more dynamically relaxed than lower- σ groups and that at least some evolved groups exist by $z \sim 0.5$.

Subject headings: gravitational lensing — galaxies: clusters: general — quasars: general — galaxies: evolution — galaxies: photometry

1. INTRODUCTION

Strong gravitational lensing of active galactic nuclei by intervening galaxies is a versatile tool for studying many astrophysical issues. Measurements of the time delay in brightness fluctuations between different images, when combined with an assumed mass model, give a measurement of the Hubble constant independent of the canonical distance ladder (e.g., Refsdal 1964; Vanderriest et al. 1989; Roberts et al. 1991; Blandford & Narayan 1992; Keeton & Kochanek 1997; Courbin, Saha, & Schechter 2002; Kochanek & Schechter 2004; Schechter 2005).

Gravitational lensing statistics can be used to constrain the density and the equation of state of dark energy (e.g., Turner 1990; Kochanek 1996a; Cooray & Huterer 1999; Chae 2003; Mitchell et al. 2005). Strong lensing also allows the determination of the mass, shape and evolution of dark-matter halos (e.g., Kochanek 1991; Keeton et al. 1998; Treu & Koopmans 2002a,b; Rusin et al. 2003; Rusin & Kochanek 2005). Anomalies in the flux ratios of individual lenses are the basis for studies of substructure in dark matter halos (e.g., Mao & Schneider 1998; Metcalf & Madau 2001; Dalal & Kochanek 2002; Metcalf et al. 2004), measurements of the size of AGN accretion disk sizes (e.g., Rauch & Blandford 1991; Wyithe et al. 2000; Yonehara 2001; Kochanek 2004) and the size of AGN broad-line regions (e.g., Abajas et al. 2002; Lewis & Ibata 2004; Richards et al. 2004).

These studies are all sensitive to the mass

Electronic address: kurtis@as.arizona.edu
Electronic address: imomcheva@as.arizona.edu
Electronic address: keeton@physics.rutgers.edu
Electronic address: aiz@as.arizona.edu
Electronic address: jlehar@combinatorx.com

¹ Present address: CombinatoRx, Inc., 650 Albany Street, Boston, MA 02118

model used to calculate the lensing potential. Understanding whether the lens potential is significantly affected by a complex environment is crucial for obtaining accurate models and avoiding significant biases (Keeton & Zabludoff 2004). Simple arguments suggest that at least 25% of lens galaxies should lie in bound groups or clusters of galaxies (Keeton, Christlein, & Zabludoff 2000), but most lens environments have not yet been studied. A few gravitational lenses are already known to lie in galaxy groups (e.g., Kundić et al. 1997a; Tonry 1998; Tonry & Kochanek 1999; Fassnacht et al. 2006) and clusters (e.g., Young et al. 1981; Fischer, Schade, & Barrientos 1998; Kneib, Cohen, & Hjorth 2000). Extended X-ray emission, indicative of more massive, dynamically evolved groups has been detected around some lenses (PG1115+080 and CLASS B1422+231; Grant et al. 2004), but not around others (CLASS B1600+434 and CLASS B1608+656; Dai & Kochanek 2005).

Attempts have been made to correlate lens models with lens environments, with mixed results (e.g., Hogg & Blandford 1994; Schechter et al. 1997; Keeton & Kochanek 1997; Kundić et al. 1997a; Kundić et al. 1997b; Lehár et al. 2000). However, these studies typically examine a region only $\sim 30''$ (~ 130 kpc at $z = 0.3$) around the lens, and group virial radii ($\sim 500h^{-1}$ kpc; Zabludoff & Mulchaey 1998) can extend out to a few arcminutes. Most recently, Momcheva et al. (2006; hereafter M06) find that six of eight lenses in that spectroscopic survey lie in groups. Some of those lenses were targeted because a group was previously known or suspected, so it is not yet clear whether M06's high group fraction is representative of most lenses. A larger, less-biased survey of lens environments is clearly required.

As gravitational lensing involves an integration of mass along the line-of-sight, one must also consider the possible effect of line-of-sight galaxy groups, both foreground and background. If the impact parameter is small and the mass large, an interloping group can have a significant impact ($\gtrsim 0.05$ in the normalized shear and convergence terms) in lensing models (M06), although theoretical estimates of whether this effect is common yield conflicting results (e.g., Seljak 1994; Bar-Kana 1996; Keeton et al. 1997; Premadi & Martel 2004). Observational studies find evidence of line-of-sight groups toward a few gravitational lenses, such as B0712+472 (Fassnacht & Lubin 2002), MG J1131+0445 (Tonry & Kochanek 2000), and B1608+656 (Fassnacht et al. 2006). In M06 we present spectroscopic identification of a massive group behind MG J0751+2716 that significantly impacts that lens model. A detailed census of line-of-sight groups is clearly needed to understand whether or not they are common, significant perturbers of lens models.

If many lenses do lie in groups, a comprehensive study of lens galaxy environments will provide a unique sample of galaxy groups with redshifts out to $z \sim 1$, the range of lens galaxy redshifts. The group environment is an important laboratory for studying galaxy evolution, as groups are common environments for galaxies and are relatively simple systems in which the range of factors impacting galaxy evolution (primarily galaxy-galaxy in-

teractions) is much narrower than in the complex, hot, dense cluster environment (Zabludoff & Mulchaey 1998). There is a small but growing number of surveys for groups at intermediate redshifts (Carlberg et al. 2001; Wilman et al. 2005; Gerke et al. 2005). These searches are challenging, because poor groups are difficult to find given their low projected surface densities and faint X-ray luminosities. The large, homogeneous sample of groups obtained from a lens survey would, when compared with local samples, permit direct observation of group evolution.

One measure of group evolution may be the properties of the brightest group galaxy (BGG). In nearby, high velocity dispersion ($\sigma \gtrsim 300 \text{ km s}^{-1}$) groups, the BGG is typically a giant, central elliptical (Zabludoff & Mulchaey 1998; van den Bosch et al. 2005). In contrast, low- σ groups at $z \approx 0$ rarely have a dominant, bright member at their centers and tend to be elliptical-poor. These results suggest that higher- σ groups are generally more dynamically evolved than their low- σ counterparts. It is unknown whether this dichotomy persists out to higher redshifts or whether group evolution is sufficiently rapid to make distant groups with central giant ellipticals rare. A sample of poor groups at higher redshift may permit this question to be addressed for the first time.

Because lensing selects on the basis of mass (e.g., Fukugita & Turner 1991), one might first expect that lens galaxies in groups would also be the BGGs. However, the sheer number of dwarf galaxies in a rich environment can offset the larger cross section of the massive BGG (Keeton, Christlein, & Zabludoff 2000), leading to the prediction that fewer than $\sim 50\%$ of lens galaxies are BGGs (Oguri 2006). Lens theory further suggests that lens galaxies span a large range of luminosities, with a typical luminosity around L_* (e.g., Kochanek et al. 2000). The data are now in hand to determine directly the distribution of lens galaxy luminosities and the fraction of lens galaxies that are also BGGs.

In order to address these issues, we have undertaken a photometric survey of ~ 80 strong gravitational lenses, nearly the complete sample of lens systems known as of early 2004, with a significant fraction of these ($\sim 1/3$) targeted for follow-up spectroscopy. The goals of our survey are to characterize the local environment of each lens galaxy out to large radii (~ 15 arcminutes), to identify any line-of-sight structures toward each lens system, to determine the impact of the local environment and the interloping systems on the lens model, and to compile a large catalog of galaxy groups at intermediate redshifts useful for studying group evolution from $z \approx 1$ to the present.

In Keeton & Zabludoff (2004), the theoretical underpinnings of the biases introduced by over-dense environments at the lens redshift are discussed in detail. In this paper we present the first results of our photometric survey, focusing on the fields of twelve lenses. Follow-up spectroscopy of eight of these lenses and detailed analyses of the shear and convergence introduced by both the immediate lens environment and any interloping structures are presented in M06. In §2 of this paper we describe the lens sample, observations, and data reduction techniques. In §3 we discuss the red-sequence finding algorithm we

use to detect candidate groups in our photometric catalog, including simulations of its effectiveness and comparisons to the spectroscopic data. In §4 we employ our sample of detected groups to address the issues raised above. Throughout this paper we assume a standard cosmology of $H_0 = 70 \text{ km s}^{-1} \text{ Mpc}^{-1}$, $\Omega_m = 0.3$, and $\Omega_\Lambda = 0.7$. Unless explicitly stated otherwise, all physical quantities from referenced papers have been adapted to this cosmology.

2. OBSERVATIONS

2.1. Sample Selection

We select our sample of twelve lens systems from the sample of all known lens systems on the basis of redshift ($z_{\text{lens}} \leq 0.5$) and foreground reddening ($E(B-V) \leq 0.2$). We also select roughly equal numbers of quadruple- and double-image lenses, as well as a handful of “other” image types (two objects with Einstein rings and one system with two lens planes). Imaging and analysis of the remaining lens systems will be presented in a future paper. The current lens sample is given in Table 1.

Of these twelve lens systems, three have previously published spectroscopically confirmed groups at the lens redshift: MG J0751+2716 (hereafter MG0751; Tonry & Kochanek 1999), PG 1115+080 (hereafter PG1115; Kundić et al. 1997a), and CLASS B1422+231 (hereafter B1422; Kundić et al. 1997a). B0712+472 (hereafter B0712) has a spectroscopic foreground group at $z \approx 0.29$ but no known group surrounding the lens (Fassnacht & Lubin 2002). Two other lens systems have either an over-density of galaxies projected around the lens (MG J1654+1346, hereafter MG1654; Langston et al. 1989) or a group identified by photometric redshifts (HE 2149-2745, hereafter HE2149; Lopez, Wucknitz, & Wisotzki 1998; Faure et al. 2004). Two more lens systems are best characterized by models including external shear, suggesting the presence of an additional mass component: BRI 0952-0115 (hereafter BRI0952; Lehár et al. 2000) and 1RXS J113155.4-123155 (hereafter RXJ1131; Sluse et al. 2003). For the remaining four lenses, FBQS J0951+2635 (hereafter FBQS0951), CLASS B1600+434 (hereafter B1600), PMN J2004-1349 (hereafter PMN2004), and CLASS B2114+022 (hereafter B2114), no evidence of a complex environment has been found previously.

It is not yet clear how representative these twelve systems are of all lens environments. This sample includes all eight lenses analyzed spectroscopically in M06, four of which were targeted there because they had known groups or good evidence for external shear. We use no information about environment to select the other four lenses in the present sample.

2.2. Data collection

We obtained observations over several observing runs between 2002 and 2004 with the Mosaic-1 imager on the KPNO Mayall 4-m telescope and the Mosaic II imager on the CTIO Blanco 4-m telescope. The observing log is given in Table 2. The wide field of view of the Mosaic cameras ($\sim 36' \times 36'$) covers the full virial radius, $r_{\text{vir}} \approx 500h^{-1} \text{ kpc} \sim 3'$, of any groups that may be present around the lens galaxies, in addition to all other massive structures that may affect the lens potential (see M06).

We imaged each field with the “nearly Mould” I filter, and with either Harris V or Harris R , with the choice of bluer filter based upon the location of the 4000\AA break at the lens galaxy redshift. We changed from V to R for $z_{\text{lens}} \geq 0.35$, approximately the redshift at which the 4000\AA break enters the R filter.²

In order to fill the gaps between the CCDs in the Mosaic cameras, we dithered the exposures. During the 2002 runs, no specific dither pattern was used; in subsequent runs we used a five-point dither pattern. We based our exposure times in 2002 (~ 1800 sec in R and I) on those necessary to obtain $S/N = 5$ at $I \approx 21.5$. Subsequently, we found this signal-to-noise to be insufficient for star-galaxy separation for $I \gtrsim 21$, and thus we increased the total exposure times to 2400–2700 secs. We split the 2002 exposures into two 900 sec exposures in each band. This strategy proved less than ideal, as the signal-to-noise in the areas affected by the chip gaps was appreciably lower, some small gaps in areal coverage remained, and the I -band sky brightness was sufficiently high (~ 11000 ADU) to fill the pixel wells to $\sim 30\%$ capacity, appreciably reducing dynamic range. In subsequent observing runs, we split the total exposure time into 480 sec or 540 sec exposures. This improved strategy increased the signal-to-noise in the chip gap regions and kept the sky levels at reasonable values.

2.3. Data Reduction

We reduced the data using the *MSCRED* package of IRAF.³ Our data reduction closely followed the prescription used by the NOAO Deep Wide-Field Survey as outlined in the online notes by Jannuzi, Claver, & Valdes.⁴ In short, we combined each night’s calibrations (bias frames, dome flats, and night-sky flats) and applied these to the science images. For KPNO data, we also created a map of the “pupil-ghost” image and subtracted this from each frame. For each night’s I -band data, we created, scaled, and subtracted fringing maps from each frame. At this point, we used coordinates from the Guide Star Catalog 2 to refine the image world coordinate systems.⁵ The images were projected onto the tangent plane and then stacked using 3σ clipping. Unlike the Deep Wide-Field Survey reduction routine, we did not remove cosmic rays in a separate step, as the σ clipping removed the vast majority of hits. We also did not fit and remove sky gradients prior to the image stacking, as the resulting stacked images were generally cosmetically better without the sky removal. We set pixels in the final stacked image that had no good values (i.e., unobserved regions, saturated pixels, and bleed trails) to an arbitrary, high value for ease of flagging in the analysis.

² We have since modified this strategy such that our ongoing survey now uses V out to $z_{\text{lens}} = 0.5$, as the V filter gives better redshift resolution than the R filter out to these larger redshifts. However, in the present paper, the $R - I$ color proves sufficient to identify groups for $0.35 \leq z_{\text{lens}} \leq 0.5$, both local to the lens and projected along the line-of-sight, as shown in §3.2.

³ IRAF is distributed by the National Optical Astronomy Observatories, which are operated by the Association of Universities for Research in Astronomy, Inc., under cooperative agreement with the National Science Foundation.

⁴ <http://www.noao.edu/noao/noodeep/ReductionOpt/frames.html>

⁵ The Guide Star Catalog was produced at the Space Telescope Science Institute under U.S. Government grant. These data are based on photographic data obtained using the Oschin Schmidt Telescope on Palomar Mountain and the UK Schmidt Telescope.

TABLE 1
 SELECTED LENS SYSTEMS

Lens Name	N_{im}^{a}	$z_{\text{lens}}^{\text{b}}$	$E(B-V)$	Obs. Night ^c			Exp. time (s)			Calib. Night ^d			References ^e
				V	R	I	V	R	I	V	R	I	
CLASS B0712+472	4	0.414	0.113	...	K1,K4	K3	...	1800	2700	1,2
MG J0751+2716	R	0.350	0.034	...	K2	K3	...	1800	2700	3,4
FBQS J0951+2635	2	0.24 ^f	0.022	K2,K3	...	K3,K4	2700	...	2700	5,6
BRI 0952-0115	2	0.41	0.063	...	C2	C3	...	1800	1800	...	C5	C5	6,7
PG 1115+080	4	0.310	0.041	C3	...	C1	1800	...	2400	SDSS	8,9,10
1RXS J113155.4-123155	4	0.295	0.035	C7	...	C7,C8	2400	...	2400	11
CLASS B1422+231	4	0.339	0.048	K1	...	K3	1800	...	2700	9,10,12
CLASS B1600+434	2	0.414	0.013	...	K2	K4	...	1800	1800	K8	2,13
MG J1654+1346	R	0.254	0.061	C2	...	C1,C2	2700	...	4500	K8	14
PMN J2004-1349	2	≤ 0.36	0.202	...	C2	C3	...	1800	1800	...	C9	C9	15,16
CLASS B2114+022	2+2?	0.316, 0.588	0.072	...	C2	C2	...	1800	1800	...	C9	C9	17,18
HE 2149-2745	2	0.495	0.032	...	C1	C1	...	1800	1800	19,20

REFERENCES. — (1) Jackson et al. 1998, (2) Fassnacht & Cohen 1998, (3) Lehár et al. 1997, (4) Tonry & Kochanek 1999, (5) Schechter et al. 1998, (6) Kochanek et al. 2000, (7) McMahon & Irwin 1992, (8) Weymann et al. 1980, (9) Kundić et al. 1997a, (10) Tonry 1998 (11) Sluse et al. 2003, (12) Patnaik et al. 1992, (13) Jackson et al. 1995, (14) Langston et al. 1989, (15) Winn et al. 2001, (16) Winn et al. 2003, (17) King & Browne 1996, (18) Augusto et al. 2001, (19) Wisotzki et al. 1996, (20) Burud et al. 2002

^aNumber of images; R indicates an Einstein Ring

^bFrom literature or CASTLES

^cSee Table 2

^dWhere necessary

^eReferences for lens discovery and lens galaxy redshift

^fPhotometric Redshift

 TABLE 2
 OBSERVING LOG

Night	UT Date	Telescope	Instrument	Seeing (")	Comments
K1	2002 March 14	KPNO Mayall 4m	Mosaic-1	1.3	...
K2	2002 March 15			1.6	...
K3	2002 March 16			1.2	...
K4	2002 March 17			1.3	cirrus; non-photometric
K8	2004 June 15	CTIO Blanco 4m	Mosaic II	1.0	...
C1	2002 May 10			0.8 – 1	...
C2	2002 May 11			1.0	non-photometric
C3	2002 May 12			1.0-1.8	non-photometric, volatile seeing
C5	2003 December 14			0.8-1.0	...
C7	2003 December 18			0.8-1.0	...
C8	2003 December 20			0.8-1.0	...
C9	2004 June 18			0.9-1.2	...

Photometric measurements — We obtained the lens field photometry using SExtractor v.2.3.2 (Bertin & Arnouts 1996). Using the image in the best-seeing band (usually I) as a reference, we shifted and scaled the stacked images for a given field with the IRAF *geotran* task. We convolved the best-seeing image with a Gaussian kernel to degrade the seeing to that of the other band.

Total magnitudes are Kron (1980) magnitudes given by the SExtractor MAG_AUTO measured from the unconvolved I -band image. We measured galaxy colors via aperture magnitudes in the matched-seeing images. We selected the aperture size to be a 6.1 kpc physical radius, equivalent to 5 pixels ($= 1''.3$) for a $z = 0.5$ galaxy. This aperture corresponds to the full width-half maximum (FWHM) of the point-spread function (PSF) in the worst-seeing lens field in this sample.

Star-galaxy separation — We tested three methods for star-galaxy separation: (1) the stellarity index output by SExtractor, which compares observed profiles with an in-

put FWHM value using a neural network algorithm, (2) χ^2 measurements output by DAOPhot (Stetson 1987), which are based on the goodness-of-fit of a model PSF, and (3) the difference in aperture magnitudes between two concentric apertures, with radii approximately equal to the FWHM and twice the FWHM. The last of these methods is motivated by the fact that point sources have a universal PSF and thus should have a constant difference in aperture magnitudes, while extended objects (galaxies) should not. We inserted artificial stars and galaxies into the PG1115+080 field using the IRAF *art-data* routine, recovered these objects with SExtractor, and performed star-galaxy separation using each of the three methods.

The DAOPhot analysis performed worst at star-galaxy separation due to the known high-frequency variations in the Mosaic PSF.⁶ The other two methods worked comparably well over a wide range of parameters, but the

⁶ See <http://www.physics.nau.edu/~pmassey/Mosaicphot.html>

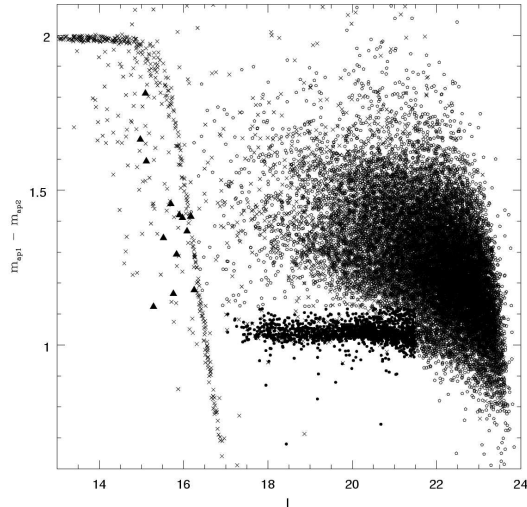


FIG. 1.— Difference in aperture magnitudes for two concentric apertures as a function of magnitude in the field of B1422. Crosses indicate objects that are flagged as saturated or have otherwise bad photometry; filled circles are objects identified as stars; open symbols are galaxies; and filled triangles are objects that we then classified by eye. A visual inspection of the saturated objects finds only one bright galaxy near the edge of the field; the other objects are either saturated or bad measurements (e.g. near the image edge, under a bleed trail, a defect, etc.). The star-galaxy separation routine works well for $16.5 \lesssim I \lesssim 21$.

aperture method was able to go slightly fainter.

The SExtractor stellarity index is a continuous parameter running from 1 for point sources to 0 for obviously extended sources, with intermediate values indicating various degrees of ambiguity. This parameter has two main drawbacks. First, it is quite sensitive to the input value of the FWHM for faint objects. Second, the value of the stellarity index corresponding to the dividing line between stars and galaxies is ill-defined. The division between stars and galaxies is subjective, and many different cuts exist in the literature.

The concentric-aperture method is illustrated in Figure 1. This method was robust over a large magnitude range, though it failed at bright magnitudes due to an ambiguity between bright extended objects and saturated stars. Although SExtractor output saturation flags, some saturated stars failed to be flagged. Therefore, we classified by eye all non-flagged objects brighter than the magnitude at which saturation set in. For most fields, this involved fewer than a dozen objects. Due to its superior ability to identify unresolved objects, we therefore used the concentric-aperture method for star-galaxy separation.

2.4. Calibrations

We calibrated our data obtained on photometric nights to the Kron-Cousins filter set using Mosaic images of Landolt standard fields (Landolt 1992). We performed multiple-aperture photometry of photometric standards using DAOPhot. Aperture corrections to infinity were calculated using the profile fitting routine DAOgrow. We assumed color transformations of the form:

$$v = V + a_0 + a_1(V - I) + a_2(X - 1.25) \quad (1)$$

$$r = R + b_0 + b_1(R - I) + b_2(X - 1.25) \quad (2)$$

$$i = I + c_0 + c_1(V - I) + c_2(X - 1.25), \quad (3)$$

where v , r , and i are the instrumental magnitudes and X is the airmass. In a few cases, depending on the bands observed during a night, the color term used in Eqn. 1 was $B - V$, and the color term used in Eqn. 3 was $R - I$; these are noted in Table 3. We assumed extinction values of $a_2 = 0.15$, $b_2 = 0.10$, and $c_2 = 0.07$ magnitudes per unit airmass for the Kitt Peak data (Massey et al. 2002), as we lacked sufficient standard star observations to determine these values. We were able to calculate extinction coefficients for each night of CTIO data. We determined color terms a_1 , b_1 and c_1 for each telescope run and made no attempt to account for known, small (millimag) chip-to-chip variations in color terms. The zero points a_0 , b_0 and c_0 were determined individually for each night. The adopted photometric coefficients are given in Table 3.

We applied the zero points and extinction coefficients to calibrate the galaxy photometry and colors but did not apply the color terms. The color terms derived above are for stellar spectral energy distributions (SEDs), which are roughly blackbody SEDs spanning a range of temperatures. The application of these color terms to colors of redshifted stellar systems was not appropriate, and at present we do not have calibrated spectrophotometry of any of our targets to determine empirical color terms for these galaxies. If we assume that these color terms are similar in size to those in Table 3, then the systematic errors we introduced into the colors would be on the order of 0.1 to 0.2 mags, similar to the size of the random errors (§2.5). For galaxies with similar spectral energy distributions at a similar redshift, such as those in the red sequence (§3.1), the systematic offset is the same for each galaxy and will not affect the detection of the red sequence. Therefore, we simply acknowledge that no color term correction has been applied to the photometry, likely introducing some small systematics into the derived colors ($\lesssim 0.1$ mags) and into the photometry-based group redshifts.

In the cases where fields were imaged on non-photometric nights, we obtained short calibration exposures of the fields on later photometric nights. We derived local standard stars in each field using aperture photometry, including appropriate aperture corrections. From these local standards we determined zero points, which include the atmospheric extinction implicitly, for each field. The fields calibrated in this manner, and the photometric nights used for calibration, are indicated in Table 1.

Special calibration steps were required for the V -band imaging of PG1115, for which we failed to obtain an image during a photometric night. Our attempts to calibrate the field with archival *HST* and archival *CFHT* data failed due to a lack of common unsaturated stars between the archival data and our field. Luckily, the PG1115 field was included in the Third Data Release of the Sloan Digital Sky Survey (SDSS DR3, Abazajian et al. 2005).⁷ We retrieved PSF magnitudes for all stellar objects within a $15'$ radius of PG1115 from

⁷ Funding for the Sloan Digital Sky Survey (SDSS) has been provided by the Alfred P. Sloan Foundation, the Participating Institutions, the National Aeronautics and Space Administration,

TABLE 3
ADOPTED PHOTOMETRIC COEFFICIENTS

Night ^a	Band	Fit Coefficients ^b			N
K1	V	$a_0 = -25.163 \pm 0.002$	$a_1 = 0.034 \pm 0.002$	$a_2 = 0.15^c$	4
	R	$b_0 = -25.369 \pm 0.005$	$b_1 = -0.052 \pm 0.006$	$b_2 = 0.10^c$	4
	I	$c_0 = -24.774 \pm 0.010$	$c_1 = -0.013 \pm 0.004$	$c_2 = 0.07^c$	3
K2	V	$a_0 = -25.101 \pm 0.007$	$a_1 = 0.034 \pm 0.002$	$a_2 = 0.15^c$	15
	R	$b_0 = -25.390 \pm 0.006$	$b_1 = -0.052 \pm 0.006$	$b_2 = 0.10^c$	10
	I	$c_0 = -24.777 \pm 0.003$	$c_1 = -0.013 \pm 0.004$	$c_2 = 0.07^c$	11
K3	V	$a_0 = -25.142 \pm 0.004$	$a_1 = 0.034 \pm 0.002$	$a_2 = 0.15^c$	4
	R	$b_0 = -25.343 \pm 0.003$	$b_1 = -0.052 \pm 0.006$	$b_2 = 0.10^c$	6
	I	$c_0 = -24.777 \pm 0.003$	$c_1 = -0.013 \pm 0.004$	$b_2 = 0.07^c$	11
K8	V	$a_0 = -25.077 \pm 0.023$	$a_1 = 0.001 \pm 0.023$	$a_2 = 0.15^c$	18
	R	$b_0 = -25.303 \pm 0.021$	$b_1 = -0.081 \pm 0.040$	$b_2 = 0.10^c$	13
	I	$c_0 = -24.732 \pm 0.017$	$c_1 = -0.031 \pm 0.016$	$c_2 = 0.07^c$	14
C1	R	$b_0 = -25.667 \pm 0.011$	$b_1 = 0.013 \pm 0.027$	$b_2 = 0.031 \pm 0.045$	8
	I	$c_0 = -24.912 \pm 0.005$	$c_1 = 0.027 \pm 0.012^d$	$c_2 = 0.000 \pm 0.022$	10
C5	V	$a_0 = -25.330 \pm 0.003$	$a_1 = 0.054 \pm 0.005$	$a_2 = 0.145 \pm 0.006$	72
	R	$b_0 = -25.517 \pm 0.003$	$b_1 = -0.022 \pm 0.006$	$b_2 = 0.097 \pm 0.006$	77
	I	$c_0 = -24.860 \pm 0.004$	$c_1 = 0.028 \pm 0.004$	$c_2 = 0.076 \pm 0.007$	73
C7	V	$a_0 = -25.307 \pm 0.004$	$a_1 = 0.036 \pm 0.003^e$	$a_2 = 0.068 \pm 0.036$	58
	R	$b_0 = -25.489 \pm 0.004$	$b_1 = -0.010 \pm 0.005$	$b_2 = 0.087 \pm 0.049$	26
	I	$c_0 = -24.829 \pm 0.006$	$c_1 = 0.027 \pm 0.004$	$c_2 = 0.065 \pm 0.072$	46
C8	V	$a_0 = -25.341 \pm 0.008$	$a_1 = 0.043 \pm 0.007^e$	$a_2 = 0.135 \pm 0.024$	39
	R	$b_0 = -25.521 \pm 0.006$	$b_1 = -0.029 \pm 0.010$	$b_2 = 0.092 \pm 0.015$	32
	I	$c_0 = -24.872 \pm 0.006$	$c_1 = 0.028 \pm 0.005$	$c_2 = 0.046 \pm 0.017$	53
C9	R	$b_0 = -25.610 \pm 0.006$	$b_1 = -0.015 \pm 0.013$	$b_2 = 0.090^c$	45
	I	$c_0 = -24.963 \pm 0.007$	$c_1 = 0.070 \pm 0.015^d$	$c_2 = 0.050^c$	23

^aPhotometric nights only

^bSee Eqns. 1 to 3

^cAdopted from published mean extinction

^dCoefficient for $R - I$

^eCoefficient for $B - V$

the SDSS DR3 database. We transformed these magnitudes to $UBVR_CI_C$ using the observed transformations given in Smith et al. (2002); we then used these magnitudes as local standards in our V and I images. The resulting zero-points were $a_0 = 25.390 \pm 0.018$ for the V -band and $c_0 = 24.947 \pm 0.052$ for the I -band. The I -band zero point was consistent with that derived from the Landolt standards, giving us confidence that the V -band calibration was accurate.

2.5. Completeness and Photometric Accuracy

We determined the completeness and photometric accuracy of the observations via artificial galaxy tests. Artificial galaxies were placed at random locations in the field, with additional artificial galaxies placed at random within $r_{\text{vir}} \equiv 500h^{-1}$ kpc of the lens galaxy. The input galaxy colors were chosen to match those expected for an early-type galaxy at the lens redshift (see Appendix A). The input magnitudes were distributed randomly and equally between $I_* - 2$ and $I = 22.5$, where I_* is the observed apparent I magnitude of an L_* galaxy located at z_{lens} (see Appendix A). For the lenses in this paper, $17.40 \leq I_* \leq 19.26$. This range includes the bulk of the galaxies in our photometric catalog.

Galaxy luminosity profiles were de Vaucouleurs ($r^{1/4}$) profiles convolved with a Gaussian kernel whose FWHM matched that measured in the image. We calculated an

effective radius from the Kormendy relation

$$\langle \mu \rangle_e = \alpha + \beta \log R_e, \quad (4)$$

where R_e is the effective radius in kpc and $\langle \mu \rangle_e$ is the average surface brightness interior to R_e in units of magnitudes per square arcsecond (Kormendy 1977). By definition, the total light within R_e is half of the total galaxy luminosity, so

$$\langle \mu \rangle_e = 2.5 \log(2\pi) + 5 \log(r_e) + m_T, \quad (5)$$

where r_e is the effective radius in units of arcseconds and m_T is the total apparent magnitude of the galaxy. Combining these two equations, setting $\beta = 3$ (the approximate value from La Barbera et al. 2003), and solving for $\log R_e$, we get

$$\log R_e = \frac{\alpha}{2} - 1.25 \log(2\pi) - \frac{5}{2} \log \theta_{\text{kpc}} - \frac{m_T}{2}, \quad (6)$$

where θ_{kpc} is the angle (in arcseconds) subtended by 1 kpc at the lens galaxy redshift. For α , La Barbera et al. (2003) give a rest-frame V -band value of

$$\alpha_V = 19.05 + 7.7 \log(1 + z_{\text{lens}}) + A_V, \quad (7)$$

where A_V is the V -band extinction. We converted this value to the observed I -band with a K -correction computed with the *symphot* tools in IRAF's *stdas* package, using the E/S0 spectrum from Coleman et al. (1980). We also applied Galactic reddening corrections interpolated from the Schlegel et al. (1998) maps using the reddening curve of Rieke & Lebofsky (1985).

We inserted the resulting artificial galaxies into each lens field and recovered them using SExtractor. Each run

included 365 artificial galaxies: 350 randomly scattered throughout the field and an additional 15 within r_{vir} of the lens. We considered an artificial galaxy recovered if its centroid was within 2.5 pixels and its I magnitude and color were within 1.0 mag of the input values. Fifty runs were performed in each lens field to build up statistics.

We plot the results from the artificial galaxy tests in a typical field (B1422) in Figure 2. Two systematic issues are readily observed. The recovered galaxy magnitudes consistently underestimated the flux, the effect being greatest for the brightest galaxies. This underestimate is due to the low surface brightness outer regions of an elliptical galaxy not being detected by SExtractor. The effect is strongest at bright luminosities because intrinsically bright ellipticals have the most diffuse surface brightness profiles. The net effect is to amplify the number of galaxies around I_* and suppress the number of galaxies brighter than $\sim I_* - 1$. For galaxies in these magnitude ranges, another method of measuring magnitudes (such as profile fitting) is necessary to accurately determine the total luminosity. Nevertheless, we did not attempt to correct the photometric catalog for these systematic magnitude offsets for two reasons. First, our method of measuring magnitudes is in common use; correcting to total magnitudes would hinder comparisons with other samples. Second, the exact offset depends on the input galaxy luminosity profile. Our tests were limited to bulge-dominated galaxies, so we could not estimate the corrections for disk-dominated galaxies. In future work we will perform detailed profile fits to the galaxies near the lens systems to address this systematic effect carefully.

For the brightest bins in the figure, the completeness is low because the central regions of bright galaxies are flagged as saturated. In order to determine if this saturation affects our results, we visually inspect objects flagged as saturated in a subset of the fields. While a handful of bright galaxies in each field are flagged as saturated, in no case are the flagged galaxies potential group members; these galaxies are either more than several arcminutes from the lens or obviously foreground, with magnitudes significantly brighter and physical extents significantly larger than any other galaxy near the lens.

Given that galaxies in groups tend to be clustered, we test whether crowding (i.e., the blending of overlapping galaxies) could be a significant source of incompleteness in our data. Overall, we find that the completeness within r_{vir} of the lens is similar to that in the remainder of the field. In some fields, such as B1422 (Figure 2), we find the completeness within r_{vir} of the lens is slightly higher than in the field as a whole. In other fields the completeness is slightly lower. These small completeness variations are most likely due to statistical fluctuations resulting from the smaller number of artificial galaxies used to calculate the completeness in the relatively small area surrounding the lens as compared to the much larger area of the complete Mosaic field. We therefore conclude that crowding is not an issue in our data.

Given the uncertainties in the model galaxies, the (ignored) scatter in the Kormendy relation, and the fact that the input artificial galaxies are solely early-type galaxies at a fixed redshift, the completeness is not necessarily valid outside the red sequence and is subject to

uncertain systematics. However, the observed field-to-field stability of the completeness, despite differing lens redshifts, seeing, and field depth, suggests that our completeness calculations are relatively robust.

3. IDENTIFYING GROUPS AND CANDIDATE GROUP MEMBERS

Due to the morphology-density relation, the early-type fraction is higher in overdense regions like groups and clusters of galaxies than elsewhere. In such cases, one observes a “red sequence” (RS) of elliptical and S0 galaxies in the color-magnitude diagram (CMD) of galaxies in the region. The RS forms the basis for our successful two-band photometric detection of galaxy groups and clusters.

Our RS detection algorithm is a modified version of that presented by Gladders & Yee (2000). Their algorithm searches color and astrometric space for localized enhancements of early-type galaxies at similar redshifts and has proven successful in locating group-mass structures over a wide range in redshift using data from optical imaging surveys. As our survey is targeted toward the immediate environment of lenses, we do not need to include the spatial filtering in our selection. The other major difference between our algorithm and that of Gladders & Yee (2000) is that we include human interaction in the selection process. While this introduces a hard-to-quantify bias into the resulting group sample, it enables us to detect less-massive groups ($\sigma \lesssim 300 \text{ km s}^{-1}$). As shown in §3.3, the resulting group catalog is nearly complete with few false detections, suggesting that any bias introduced by the human interaction is small.

3.1. Group Detection

Our basic RS detection algorithm is as follows. First we search within r_{vir} of the lens galaxy for an excess of galaxies with similar colors above the measured background color distribution. We fit an RS to these galaxies, and calculate the projected spatial centroid of the candidate group. Using the RS fit and centroid, we repeat this search to ensure that the group is not spurious and to refine the RS parameters and centroid measurement. We continue the iterative process until the changes in the centroid and the RS parameters are within the calculated errors. The first time we apply this algorithm to a field, we focus on galaxy colors near that of an early-type galaxy at the lens redshift, z_{lens} . We then search for line-of-sight groups by repeating the algorithm until we have investigated all peaks in the initial color distribution.

We assume an RS of the form

$$(V - I)_0 = (V - I)_* - \beta_V(I_0 - I_*), \quad (8)$$

where β_V is the slope of the RS, and $(V - I)_*$ is the unreddened observed $V - I$ color of an L_* galaxy at the lens redshift. For fields with R -band imaging, we use this same relation with V replaced by R .

We allow both the RS slope β_V and the group redshift, which determines I_* and $(V - I)_*$, to vary freely. We calculate the initial $(V - I)_*$ and I_* from the galaxy models described in Appendix A and the known z_{lens} . The RS slope has been found to have values around $d(U - V)/dM_V = 0.08$ (e.g., Bower et al. 1992; Bell et al. 2004;

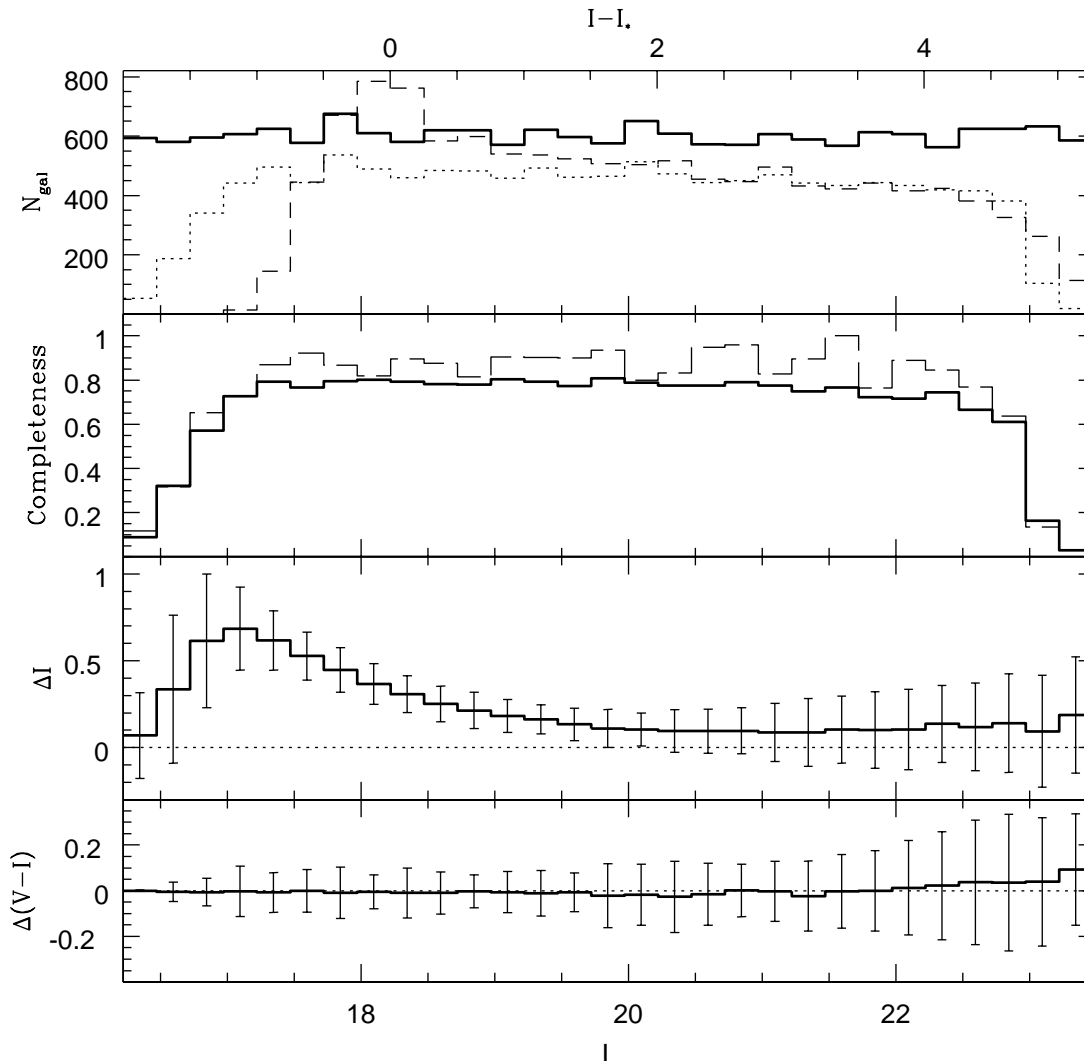


FIG. 2.— Results of artificial galaxy tests in the field of CLASS B1422+231 (hereafter B1422). The top panel shows the number of artificial galaxies (over all 50 runs) as a function of input total magnitude for all galaxies (heavy solid line) and all recovered galaxies (dotted line), as well as the number of recovered galaxies as a function of *measured* magnitude (dashed line). The second panel shows the completeness as a function of input total magnitude for the entire image (heavy solid line) and the region within a $500h^{-1}$ kpc projected radius of the lens (dashed line). The third panel shows the mean difference between the total magnitude and the measured magnitude as a function of total magnitude; error bars give the 1σ deviation about the mean. The bottom panel shows the mean difference between the input and measured aperture colors as a function of total magnitude; error bars are the 1σ deviation about the mean.

McIntosh et al. 2005). Because the color-magnitude relation is difficult to model properly, and because our bandpasses do not correspond exactly to rest-frame U and V , it does not necessarily follow that this slope can be directly compared with the $V - I$ or $R - I$ slopes of the groups in this paper. However, we show in §4.1.1 that the actual fit slopes from our sample are indistinguishable from this value. We therefore initially set $\beta_V = 0.08$. Although this could bias the final fit slopes, we show in §3.2 that we can recover the correct RS slope even if this initial assumed value is incorrect.

For the first iteration of our RS search, we limit the search to within $r_{\text{vir}} (= 500h^{-1}\text{kpc})$ of the lens galaxy. This radius is large enough ($\sim 2'-3'$) to include most of the line-of-sight structures that could impact lens models

(see M06). It is possible that a massive galaxy cluster could lie outside this radius and still alter the lens potential, so we estimate the fraction of lenses affected by such a cluster as follows. We consider a lens model perturbation significant if the convergence $\kappa \geq 0.05$. From Eqn. A20 in M06, we find that the maximum impact parameter b_{max} that a cluster can have and significantly impact the lens model is $b_{\text{max}} = 4.8 \times 10^{-6} \sigma^2$, where b_{max} is in arcminutes and σ is the cluster velocity dispersion in km s^{-1} . This conservatively assumes that the cluster is at the lens redshift; for clusters at other redshifts, b_{max} will be smaller. For a galaxy cluster with $\sigma \sim 750 \text{ km s}^{-1}$, the median velocity dispersion for rich Abell clusters (Zabludoff, Huchra, & Geller 1990), $b_{\text{max}} \approx 3'$ — close to the radius within which we search anyway. The

surface density of galaxy clusters is ~ 11 per sq. degree (Gonzalez et al. 2001, $0.3 \lesssim z_{\text{cluster}} \lesssim 0.9$, correcting for their 30% false detection rate). On average, this results in 0.07 galaxy clusters within b_{max} . We consider this to be an upper limit, given that we are already searching for groups and clusters out to a significant fraction of b_{max} and that b_{max} is smaller if there is any redshift difference between the cluster and the lens. We therefore conclude it is unlikely that any significant perturbing structures lie outside our search radius.

We correct galaxy magnitudes for interstellar extinction and reddening using standard Galactic extinction (Rieke & Lebofsky 1985) with $R_V = 3.1$ and extinctions from Schlegel et al. (1998) obtained from the NASA Extragalactic Database.⁸ We do not attempt any corrections for differential Galactic extinction across the field; any variations within r_{vir} of the lens are likely to be negligible at the Galactic latitudes of these lenses. As is common practice, extinction-corrected magnitudes and colors are denoted by the subscript “0.”

To account for the slope of the RS, we define an “effective color” for each galaxy:

$$(V - I)_{\text{eff}} = (V - I)_0 + \beta_V(I_0 - I_*). \quad (9)$$

This represents the color each galaxy would have if it resided on the RS and had an apparent magnitude $I = I_*$. This definition is useful because all RS galaxies in a group should have the same effective color. Hence, we can identify RSs as peaks in a histogram of effective color, providing an efficient way of searching for groups of early-type galaxies. The search for peaks in the effective color histograms is also adept at identifying groups with high late-type fractions, as blue galaxies in a group will all have roughly similar colors, although in the absence of morphological or spectroscopic data to classify the galaxies as late-types, the derived redshift of the group will be incorrect (see §3.2).

We compute effective color histograms for galaxies within r_{vir} of the lens galaxy, as well as for all galaxies in the image (normalized to the area within r_{vir}). The number density of field galaxies as a function of apparent magnitude has a steeper slope than typical group luminosity functions (e.g., Lin et al. 1999; Gladders & Yee 2000), so it is possible to choose a magnitude limit that maximizes the contrast between the RS and the field galaxy distribution. This magnitude limit will vary from field to field depending on the richness of the group and statistical fluctuations in the number of background galaxies. Our empirical testing finds that, in most cases, the best contrast between the group and the field is achieved for a limiting magnitude of $I \approx I_* + 2.5$. We therefore consider only galaxies brighter than $I_* + 2.5$ throughout this algorithm.

We visually examine the effective histograms for an excess of galaxies of a similar effective colors relative to the normalized field background, an indication of a possible group. We select all galaxies within a distance $\Delta(V - I)_{\text{eff}}$ of the peak in the effective color histogram as candidate RS galaxies. We take $\Delta(V - I)_{\text{eff}}$ to be the larger

of the photometric color error and 0.05 mags, the typical RS scatter in the literature (e.g., Bower et al. 1992; McIntosh et al. 2005). The photometric color errors are typically larger than the intrinsic scatter for $I \gtrsim 21$.

We use linear regression to fit a linear RS to the selected galaxies brighter than $I_* + 2.5$, thereby refining the RS slope β_V and intercept. From this fit we determine the new values of $(V - I)_*$, I_* , and the RS redshift z_{RS} based on the early-type galaxy photometric models (Appendix A). As discussed in Appendix A, we note that changes in the assumed normalization of I_* results in systematic changes in z_{RS} , though for the range of published values of L_* , this bias is $\Delta z_{\text{RS}} \leq 0.02$. We also calculate the raw and luminosity-weighted group centroids of the RS galaxies.

At this point, we can either accept or reject the new parameter values and then choose whether another iteration should be performed. Changes in redshift cause the projected angular size of r_{vir} to be recomputed, and changes in the centroids adjust the area of sky in which galaxies are examined. The iterative process continues until the change in the RS redshift between iterations is less than $\Delta z_{\text{RS}} = 0.02$ and the shift in the centroid is less than 1σ . If multiple peaks in the color distribution are observed, we repeat the entire process on each potential RS. For the purpose of this paper, we define “significant” candidate RSs as those with at least three selected galaxies above the averaged background persisting for at least two iterations, criteria that produce the best results in tests with mock groups (see §3.2).

An example of this process applied to the lens B1422 is shown in Figure 3. We see an RS of galaxies at $V - I \approx 1.9$, roughly the effective color of early-type galaxies at z_{lens} and also the approximate color of the lens galaxy. At brighter magnitudes, the group luminosity function clearly dominates that of the field. A map of the galaxies in this range (Fig. 3c) shows that the collection of bright galaxies, and therefore the group, is nearly centered on the lens galaxy and is elongated. This figure shows that our group detection algorithm is capable of detecting physical groups and constraining the group redshift, richness, centroid, and shape. We note that some of the bright galaxies in the selected RS may not be group members but rather higher-redshift blue galaxies. In the future, we will also perform a morphological analysis, which should separate background disk-dominated galaxies from the early-type RS group members. For now, we make two tests of the algorithm, one using simulated groups of galaxies (§3.2), the other using spectroscopy of eight of the twelve lens fields to verify RS membership (§3.3).

3.2. Testing the Algorithm: Simulated Data

We test our RS search algorithm by inserting mock galaxy groups into each field’s galaxy catalog. We construct mock photometric groups from empirical luminosity functions. The early-type fraction and number of bright group galaxies are readily modified to simulate galaxy groups of different richnesses. The precise luminosity function does not significantly affect the success of the algorithm.

We begin by creating a mock group galaxy catalog designed to cover a range of redshifts ($z = 0.2, 0.4, 0.6$), early-type fractions ($f_e = 0.0, 0.5, 1.0$), RS slopes

⁸ This research has made use of the NASA/IPAC Extragalactic Database (NED) which is operated by the Jet Propulsion Laboratory, California Institute of Technology, under contract with the National Aeronautics and Space Administration.

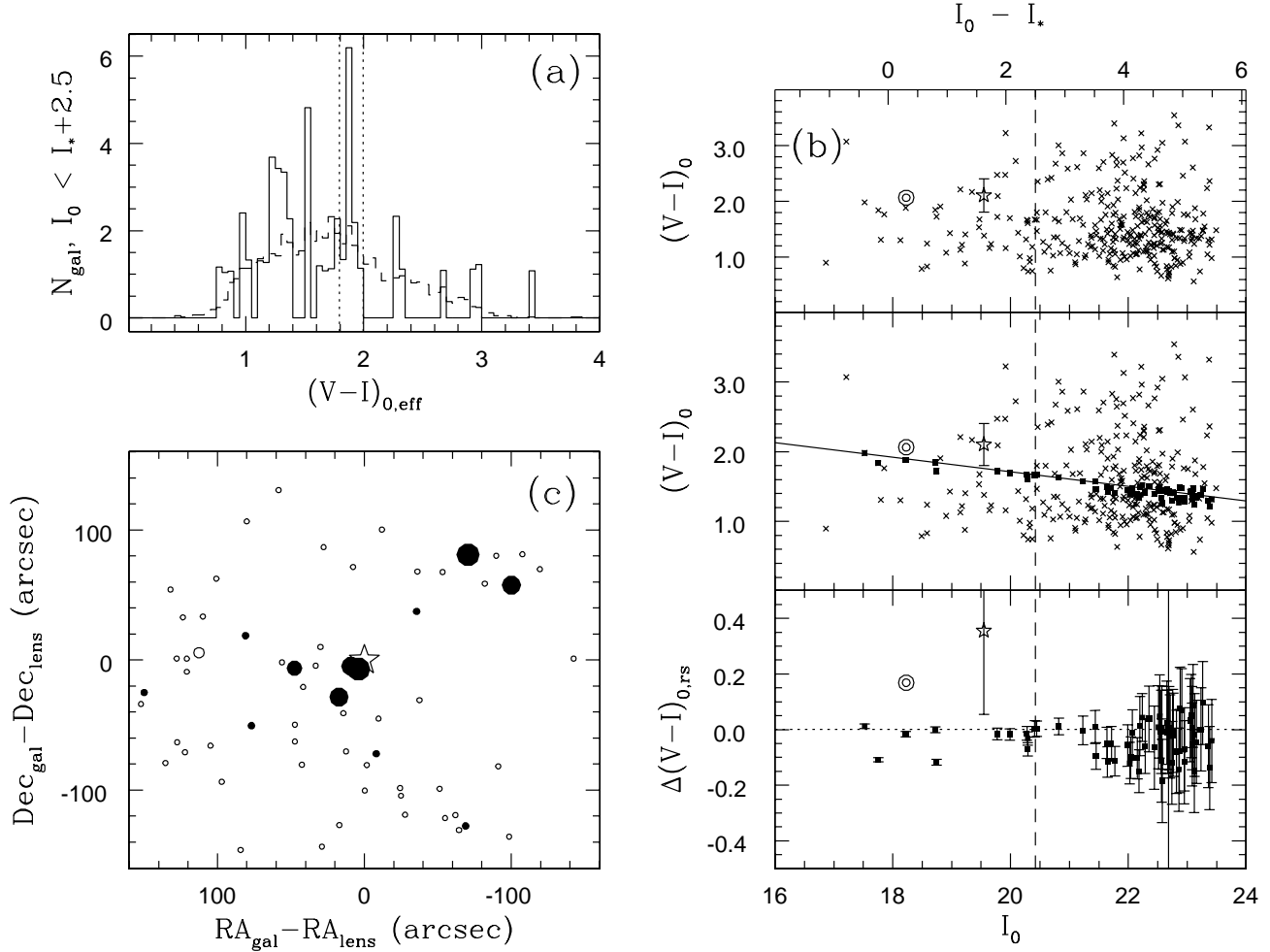


FIG. 3.— Illustration of our group-finding algorithm for B1422. (a) Histograms of effective colors for galaxies brighter than $I_* + 2.5$ projected within r_{vir} (solid) and for the entire field normalized to the area within r_{vir} (dashed). Vertical dotted lines bracket the region in $(V-I)_{\text{eff}}$ from which the final group member catalog was selected. (b, top panel) Color-magnitude diagram for all galaxies (crosses) projected within r_{vir} . The star with error bars indicates the lens galaxy; concentric circles indicate the expected location of an L_* early-type galaxy at the lens redshift. (b, middle panel) Color-magnitude diagram for galaxies projected within r_{vir} (crosses) with galaxies selected by the red sequence finding algorithm shown as filled boxes. The solid line is the fit red sequence. The vertical dashed line in all right-hand panels indicates the faint magnitude limit of the final red-sequence fitting. (b, bottom panel) Residuals of the selected red sequence candidates about the best-fit line. Error bars indicate errors estimated from the artificial galaxy tests. (c) Map of red sequence-selected galaxies projected within r_{vir} as a function of distance from the lens galaxy (open star). Filled circles indicate galaxies brighter than $I_* + 2.5$ and are larger for brighter objects. This figure illustrates the ability of the red sequence finding algorithm to locate physical groups.

($\beta_V = 0.05, 0.10, 0.15$), and richnesses. We define the mock group richness by the number of galaxies brighter than $I_* + 2$, and our mock groups are designed to have richnesses of 4, 8, or 16. A richness of 4 corresponds to Local Group analogues. We derive cumulative luminosity functions from the empirical group luminosity functions presented in Zabludoff & Mulchaey (2000) to determine that richnesses of 8 and 16 correspond to velocity dispersions of $\sigma_v \sim 300 \text{ km s}^{-1}$ and $\sigma_v \sim 500 \text{ km s}^{-1}$, respectively, though there is significant scatter in this relation.

We select the luminosity function for each group from the empirical luminosity functions derived from GEMS data (Miles et al. 2004). That study presents different luminosity functions for X-ray bright ($L_x \geq 10^{41.7} \text{ erg s}^{-1}$) and X-ray faint/undetected groups. This luminosity break corresponds to a velocity dispersion of $\sim 200 \text{ km s}^{-1}$ (Mulchaey & Zabludoff 1998), so we use the GEMS

empirical X-ray faint luminosity function for groups with richness 4 and the X-ray bright luminosity function for groups with richness 8 or 16.

We assign each mock galaxy an I magnitude drawn randomly from a distribution defined by the appropriate luminosity function. We then label each galaxy an early- or late-type with a probability based on the input early-type fraction (f_e). Late-type galaxies are further divided with equal probability into Sa, Sb, and Sc types. We assign colors based on the appropriate photometric model (Appendix A) for the assigned morphology, and, for early-types, we place the galaxy on the RS with a selected RS slope between $\beta_V = 0.05$ and 0.15. We add Gaussian scatter of $\sigma_{V-I} = 0.05 \text{ mag}$, similar to the observed scatter in other RS studies, to each mock galaxy's color. We also add additional scatter to the I magnitude and color of each galaxy to simulate the photometric er-

rors based on the photometric accuracy determined from the artificial galaxy tests (§2.5).

We now need to assign positional data to each galaxy. To simulate the foreground and background galaxies in the field, we assign the cataloged galaxies random x - and y -positions in the B1422 field (chosen to be a representative lens field), thereby mixing any actual galaxy groups and clusters into the field galaxy population. We assume that all mock group galaxies lie within r_{vir} of the lens, and we assign these galaxies positions drawn randomly from a 2-dimensional Gaussian density function centered on the lens position. We then run the group finding algorithm on the combined catalog. We consider a mock group to be recovered if we find a candidate RS with an effective color within 0.2 of the input group’s color, a value similar to our input color errors. This criterion prevents the detection of spurious groups, i.e., those containing none of the input mock galaxies. We make an exception to this criterion if the group has a high late-type fraction, in which case there often is a false RS created by having many blue galaxies with similar colors. In this circumstance, the group is considered recovered despite having an effective color >0.2 mag bluer than that of a true RS at the group redshift. In group catalogs based on our actual data, groups with high late-type fractions would be labeled line-of-sight groups.

Our knowledge of the mock group color could potentially bias the group finding algorithm toward detection of the mock group. However, we also know the redshifts (and therefore expected RS colors) of the lenses in the present sample, so any bias for detecting groups at z_{lens} and the mock groups is the same. The small number of interloping groups identified from spectroscopy that are undetected photometrically (see §3.3) argues that this bias is also small for line-of-sight group detection. The results of the simulations are given in Table 4.

These tests indicate that we can detect rich groups via our detection algorithm out to the highest lens redshifts in our sample, independent of f_e . Groups with velocity dispersions of ~ 300 km s $^{-1}$ are detectable out to $z \approx 0.4$, although by $z = 0.6$ the detection rate is quite low ($\lesssim 50\%$). Local Group analogs are detectable at the $\sim 50\%$ level at low redshifts ($z = 0.2$) if f_e is close to one or to zero, although the former case is unlikely to occur given that the early-type fractions of the poorest groups are small (Zabludoff & Mulchaey 1998). The detection rate of the Local Group analogues at $z \geq 0.4$ is consistent with the false-detection rate (see below). We are therefore confident that we can reliably detect the majority of galaxy groups with velocity dispersions $\gtrsim 200$ – 300 km s $^{-1}$ out to $z = 0.4$. We can detect poorer groups out to $z \approx 0.2$.

From the simulations we learn that, in the absence of morphological information, the fit RS colors are systematically bluer than the input value. The reason is that some late-type galaxies (typically Sa’s) are included in the sample when the RS is fit. For systems with f_e near 1, the error is small. In the groups with low f_e , we observe a broad peak in the effective color distribution due to the late-type galaxies, and the estimated group redshift is biased low (the magnitude of this bias is redshift dependent). We could lessen this systematic effect by including morphological information in our galaxy selection; in future work we will use galaxy profile fitting

software (e.g., *GIM2D*; Simard et al. 2002) to reject disk-dominated systems from the sample used to fit the RS. Even without this morphological information, we determine group redshifts with reasonable accuracy (see §3.3).

We note that the individual fit RS slopes are very noisy and imprecise, although the ensemble average is relatively accurate. For groups with $f_e \approx 1$, the individual slope measurements are much more accurate (Table 4). This suggests that the accuracy of the slope determinations would be greatly improved by using morphological data to exclude late-type galaxies from the RS fit.

Finally, we note that the measured scatter about the RS is not a reliable measure of the input scatter. For groups with $I_* + 2.5 \gtrsim 20$ ($z > 0.25$), the photometric color errors dominate the RS scatter. By contrast, for groups with few RS members, the paucity of red sequence galaxies results in an artificially low scatter. Only for richness 16 groups at low redshifts ($z \leq 0.25$) is the recovered scatter comparable to the input scatter.

False positives — To determine the rate of false positives, we run the group-finding algorithm on two lens fields, B1422 (for $V - I$) and MG0751 (for $R - I$). We assign each galaxy in the photometric catalog a new, random position in the field, thereby washing out any true groups and clusters. We then search for peaks in the effective color histogram, both within 0.05 mags of the lens galaxy color (the typical scatter about the input color in the mock RSs), simulating false positive detections of lens groups, and at other colors, simulating false line-of-sight structures. Fifty such runs are performed in each field.

For the $V - I$ data, we record only two (i.e., 4%) false positive detections of lens galaxy groups and eight (16%) false positive line-of-sight groups. For the $R - I$ data, 12 fields (24%) have false positive lens galaxy groups, and six (12%) have false positive line-of-sight groups. The higher number of false positives in the $R - I$ data arises mainly from the smaller color range spanned by the catalog galaxies (~ 2 mags, compared to ~ 4 mags in $V - I$). Each color bin therefore contains more field galaxies, and the Poisson fluctuations often exceed the group threshold. The rate of false positive lens groups in the MG0751 field is also enhanced by the fact that the expected RS color at z_{lens} ($R - I = 0.91$) lies near the peak of the field galaxy color distribution, so shot noise from the field population is even larger. This latter problem vanishes for R -band lens fields where $(R - I)_* \gtrsim 1$, or $z_{\text{lens}} \gtrsim 0.45$, as the field density of galaxies at these colors is much lower.

As a whole, false positives are not a serious concern for the lenses in our sample with V band imaging. For lenses with R -band imaging, we need to account for the false positive rate, especially for lower-redshift lenses where the $R - I$ colors are similar to that of the majority of background galaxies. As will be shown in §4.1.1, these false positives have a minimal impact on our conclusions.

3.3. Testing the Algorithm: Spectroscopic Confirmation

The ultimate test of the group finding algorithm is whether the candidate groups can be confirmed as real, bound systems. We have obtained spectroscopic redshifts of ~ 100 galaxies in each of eight lens fields (MG0751, BRI0952, PG1115, B1422, MG1654, PMN2004, B2114, and HE2149); the identification of bound systems and the analysis of their impact on lens-

TABLE 4
RESULTS FROM GROUP-FINDING ALGORITHM TESTS WITH MOCK GROUPS

z (1)	f_e (2)	N_{I_*+2} (3)	β_V (4)	N_{rs} (5)	$\overline{N}_{I_*+2, det}$ (6)	$\overline{\Delta\beta_{V, fit}}$ (7)	$\overline{\Delta(V-I)_{*, fit}}$ (8)	Scatter (9)
0.2	1.00	16	0.05	5	13.3 ± 3.2	0.023 ± 0.022	-0.011 ± 0.015	0.065 ± 0.019
			0.10	5	14.1 ± 2.4	0.005 ± 0.014	-0.027 ± 0.019	0.080 ± 0.015
			0.15	5	14.4 ± 2.5	-0.014 ± 0.011	-0.022 ± 0.012	0.067 ± 0.025
		8	0.05	4	6.5 ± 1.0	0.017 ± 0.044	0.008 ± 0.027	0.079 ± 0.016
			0.10	3	6.8 ± 3.2	-0.038 ± 0.046	0.001 ± 0.029	0.008 ± 0.002
			0.15	4	6.0 ± 1.6	0.009 ± 0.043	-0.007 ± 0.013	0.005 ± 0.002
	0.00	4	0.05	1	10.6	0.028	0.030	0.007
			0.10	3	3.9 ± 1.1	-0.026 ± 0.032	-0.036 ± 0.015	0.097 ± 0.012
			0.15	0
		16	...	5	10.7 ± 4.8	0.062 ± 0.053	-0.184 ± 0.013	0.010 ± 0.005
			...	4	5.2 ± 1.0	0.047 ± 0.034	-0.179 ± 0.020	0.013 ± 0.006
			...	3	3.2 ± 1.0	0.104 ± 0.020	-0.186 ± 0.008	0.019 ± 0.004
0.50	16	0.10	5	7.8 ± 2.9	-0.001 ± 0.008	-0.047 ± 0.024	0.011 ± 0.004	
		0.10	3	5.4 ± 0.9	-0.029 ± 0.014	-0.052 ± 0.043	0.017 ± 0.004	
		0.10	1	4.6	0.012	0.030	0.011	
	4	0.05	5	15.2 ± 3.9	0.026 ± 0.023	-0.017 ± 0.016	0.107 ± 0.017	
		0.10	5	17.6 ± 3.1	0.000 ± 0.010	-0.011 ± 0.016	0.087 ± 0.027	
		0.15	5	16.2 ± 2.2	-0.001 ± 0.027	-0.023 ± 0.013	0.088 ± 0.032	
0.4	1.00	8	0.10	5	7.9 ± 2.2	0.017 ± 0.027	-0.017 ± 0.016	0.118 ± 0.026
			0.10	3	5.2 ± 3.1	0.024 ± 0.054	-0.031 ± 0.054	0.146 ± 0.014
			0.10	4	8.4 ± 2.3	0.034 ± 0.043	-0.178 ± 0.219	0.102 ± 0.026
	0.50	8	0.10	4	5.3 ± 1.8	0.000 ± 0.067	-0.244 ± 0.249	0.125 ± 0.014
			0.10	1	3.1	-0.041	-0.538	0.105
			0.10	5	10.1 ± 4.0	0.121 ± 0.048	-0.441 ± 0.074	0.107 ± 0.037
0.00	16	...	4	7.6 ± 2.8	-0.013 ± 0.028	-0.527 ± 0.057	0.108 ± 0.008	
		...	4	
		...	0	
	8	0.05	5	12.0 ± 3.4	0.014 ± 0.016	-0.009 ± 0.008	0.109 ± 0.027	
		0.10	5	12.0 ± 3.6	0.007 ± 0.035	-0.009 ± 0.016	0.101 ± 0.026	
		0.15	5	10.3 ± 1.7	0.002 ± 0.036	-0.001 ± 0.020	0.107 ± 0.035	
0.6	1.00	8	0.10	1	4.8	0.002	-0.029	0.097
			0.10	0
			0.10	3	9.8 ± 5.7	0.009 ± 0.037	-0.010 ± 0.022	0.130 ± 0.009
	0.50	8	0.10	2	5.1 ± 0.9	-0.019 ± 0.018	-0.336 ± 0.474	0.124 ± 0.001
			0.10	2	3.4 ± 0.1	0.003 ± 0.054	-0.650 ± 0.030	0.108 ± 0.013
			0.10	4	8.8 ± 4.0	0.044 ± 0.088	-0.507 ± 0.088	0.109 ± 0.020
0.00	16	...	3	4.1 ± 0.9	0.041 ± 0.039	-0.588 ± 0.000	0.114 ± 0.004	
		...	2	5.6 ± 1.9	0.006 ± 0.018	-0.716 ± 0.289	0.102 ± 0.035	

NOTE. — (1) Redshift of input group (2) Early-type fraction of input group (3) Number of input galaxies brighter than $I_* + 2$ (4) Input RS slope (5) Number of mock groups recovered (6) Mean number of recovered galaxies in RS (7) Mean recovered RS slope (8) Mean offset of RS effective color from input effective color (9) Mean scatter about fit RS

ing are discussed in M06. The group-finding algorithm detects eleven groups in these eight fields, both at z_{lens} and elsewhere along the line of sight. Overall, the group finding algorithm works exceptionally well, with ten of the eleven candidate groups confirmed spectroscopically (Table 5). The lone exception is the RS at $z_{RS} = 0.20$ in the foreground of the PG1115 lens. While Figure 3 in M06 shows a potential peak at this redshift, there are too few velocities to determine if the peak is real. We also do not recover two spectroscopic line-of-sight groups in our photometry. The spectroscopic group in B1422 at $z = 0.28$ is blended with the lens group RS in color space, while the HE2149 group at $z = 0.27$ simply is not detected.

The photometric redshifts tend to be slightly lower than the spectroscopic redshifts ($\overline{\Delta z} = -0.02 \pm 0.04$), because the group finding algorithm tends to return colors that are slightly bluer than the true RS, as discussed in §3.2. This offset is small, which shows that our photometric group finding algorithm obtains reliable redshifts for detected groups of galaxies.

Figure 4 shows the spectroscopic group members and non-members in comparison with the fit RS for B1422. The fit RS agrees with the red edge of the envelope defined by the group members. Figure 5 shows the spectroscopic group members and fit RSs for both the lens group and a background group in PG1115. The background group in PG1115 has a significantly higher spectroscopic redshift ($z_{sp} = 0.486$) than the photometric RS redshift ($z_{RS} = 0.41$), suggesting that this group may have a low f_e ; indeed, M06 find that six of the ten confirmed group members have emission lines. Both of these figures illustrate the success of our RS finding technique.

We define a red-sequence richness parameter N_{RS} to be the number of selected RS galaxies brighter than $I_* + 2.5$ over and above the normalized background. With two-band photometry alone, this is the best richness measure we can make. We compare N_{RS} with the measured velocity dispersions from M06. Contrary to expectations, we find no significant correlation. The explanation may be that variable early-type fractions and statistical background noise add significant scatter (see also the large

TABLE 5
PARAMETERS OF SIGNIFICANT CANDIDATE RED SEQUENCES

RS ID ^a	z_{RS}	z_{spec}	I_*	$(V-I)_*$	$(R-I)_*$	RS Slope	N_{RS}	RS Scatter
B0712 : GROUP 1	0.63	...	19.903	...	1.361 ± 0.029	0.115 ± 0.029	9.2	0.088
MG0751: GROUP 1	0.34	0.3502	18.229	...	0.900 ± 0.051	0.093 ± 0.032	5.8	0.044
MG0751: GROUP 2	0.48	0.5605	19.149	...	1.087 ± 0.037	0.121 ± 0.023	13.1	0.047
FBQS0951: GROUP 1	0.16	...	16.461	1.434 ± 0.060	...	0.052 ± 0.042	5.6	0.038
FBQS0951: GROUP 2	0.27	0.24 ^b	17.675	1.770 ± 0.041	...	0.062 ± 0.032	5.8	0.047
FBQS0951: GROUP 3	0.43	...	18.844	2.349 ± 0.037	...	0.034 ± 0.024	6.4	0.051
BRI0952: GROUP 1	0.37	0.4220	18.441	...	0.938 ± 0.057	0.059 ± 0.048	8.4	0.020
PG1115: GROUP 3	0.26	...	17.587	1.732 ± 0.162	...	0.063 ± 0.081	4.7	0.038
PG1115: GROUP 1	0.30	0.3101	17.924	1.895 ± 0.045	...	0.078 ± 0.017	3.4	0.031
PG1115: GROUP 2	0.41	0.4859	18.713	2.297 ± 0.077	...	0.116 ± 0.042	3.4	0.080
RXJ1131: GROUP 1	0.19	$\approx 0.104^c$	16.864	1.508 ± 0.024	...	0.059 ± 0.020	25.6	0.045
RXJ1131: GROUP 2	0.29	0.295 ^b	17.844	1.852 ± 0.077	...	0.071 ± 0.046	6.2	0.056
B1422: GROUP 1	0.30	0.3387	17.924	1.895 ± 0.049	...	0.104 ± 0.031	6.0	0.054
B1600: GROUP 1	0.50	...	19.262	...	1.123 ± 0.064	0.086 ± 0.041	12.1	0.035
MG1654: GROUP 1	0.22	0.2527	17.204	1.596 ± 0.046	...	0.079 ± 0.033	4.8	0.021
B2114: GROUP 1	0.26	0.3144	17.587	...	0.792 ± 0.058	0.055 ± 0.030	7.0	0.062
HE2149: GROUP 3	0.40	0.4465	18.647	...	0.968 ± 0.060	0.047 ± 0.036	5.6	0.052
HE2149: GROUP 4	0.59	0.603	19.720	...	1.288 ± 0.068	0.086 ± 0.042	5.3	0.041

NOTE. — The IAU-approved naming convention for these groups is Lens Name: MWKZ GROUP N, where N is the group ID; e.g., CLASS B0712+472: MWKZ GROUP 1

^aMatched to M06 where applicable

^bNo group data in M06; lens galaxy redshift from Table 1

^cRedshift of BRSG from Las Campanas Redshift Survey (Shectman et al. 1996)

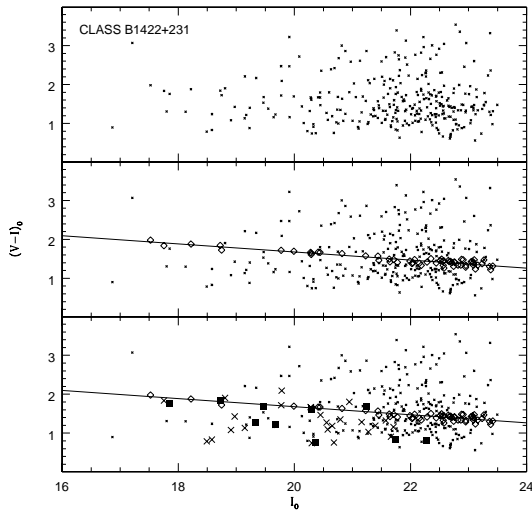


FIG. 4.— Comparison of RS-finding algorithm with spectroscopic data for B1422. *Top panel:* Extinction-corrected color-magnitude diagram for all galaxies (small crosses) within a projected r_{vir} radius surrounding the centroid of the B1422 group. *Middle panel:* Same as top panel, but with best-fitting RS (solid line) and selected candidate RS-member galaxies (open diamonds) shown. *Bottom panel:* Same as middle panel, but with spectroscopically confirmed group members from M06 (filled squares, including galaxies from beyond r_{vir}) and confirmed non-members (large crosses) shown. This figure shows that the fit RS agrees with the red edge of the envelope defined by the spectroscopically-confirmed group members.

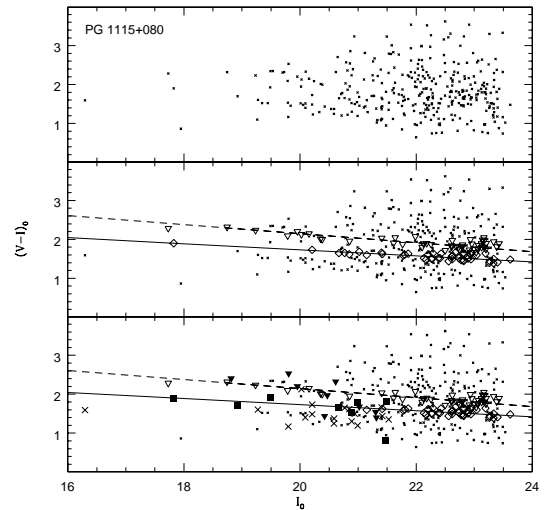


FIG. 5.— Same as Figure 4, but for PG1115. Open triangles (center and bottom panels) indicate the candidate RS member galaxies for the background group; filled triangles (bottom panel) indicate spectroscopic members of the background group. The dashed line indicates the fit RS for the background group. This figure illustrates the ability of the red-sequence finding algorithm to detect multiple groups in a given field.

4. RESULTS AND DISCUSSION

4.1. The Detected Red Sequence Sample

scatter in N_{*666} versus σ for 2MASS galaxy clusters with $\sigma \lesssim 500 \text{ km s}^{-1}$; Kochanek et al. 2003). The full sample of groups from our complete survey will overcome this issue by spanning a much larger dynamic range, making the comparison between N_{RS} and σ more meaningful.

In total, eighteen significant candidate RSs are detected in twelve lens fields in the present sample. The fit RS parameters are presented in Table 5, and the photometry of the selected galaxies is presented in Table 6 (available electronically).

Although some final centroids lie outside r_{vir} of the

TABLE 6
PHOTOMETRY OF CANDIDATE RED SEQUENCE GALAXIES

Lens	Group ID	Galaxy ID	RA	Dec	I	δI	$R - I$	$\delta(R - I)$
B0712	1	8471	07 16 04.35	47 08 59.2	18.61	0.03	1.60	0.03
B0712	1	9253	07 15 56.86	47 09 23.7	20.80	0.03	1.45	0.07
B0712	1	9109	07 15 58.92	47 08 52.3	20.82	0.03	1.45	0.01
B0712	1	9412	07 15 55.16	47 09 53.5	21.21	0.05	1.27	0.11
B0712	1	8204	07 16 09.09	47 10 04.5	21.28	0.05	1.10	0.20

NOTE. — (1) Full table is available electronically. (2) The IAU-approved naming convention for individual galaxies is: Lens Name: MWKZ GAL NNNN, where NNNN is the galaxy ID above; e.g., B0712+472: MWKZ GAL 8471. (3) Units of right ascension are hours, minutes, and seconds, and units of declination are degrees, arcminutes, and arcseconds (J2000.0).

lens, we initially detected each RS peak within r_{vir} of the lens galaxy. It is certain that the wide-field images contain additional structures outside of this initial search radius; no attempt has been made so far to locate such structures.

The average RS slope, $\Delta(V-I)/I$ or $\Delta(R-I)/I$, for all 18 candidate groups is 0.076 ± 0.025 . This scatter is comparable to that measured in the mock groups (Table 4), so there is no evidence that the RS slope is anything but universal at these moderate redshifts. We note that these slopes are not corrected for redshift/evolutionary effects. Such a correction would require a detailed understanding of the origin of the RS and its redshift evolution.

4.1.1. The Fraction of Lenses in Complex Environments

Of the twelve lens systems in this paper, eight have significant red sequences within $\Delta z = 0.06$ of the lens redshift. Of these systems, six were known or suspected previously to have a group at the lens redshift due to the need for shear in the lens models or to an overdensity of galaxies on the sky surrounding the lens. The two new systems are FBQS0951 ($z_{\text{RS}} = 0.27$) and B2114 ($z_{\text{RS}} = 0.26$); the B2114 group has been confirmed spectroscopically (M06).

Figure 6 shows the CMDs for each of the twelve lens fields. In the cases where an RS is detected at the lens redshift, the fit RS and the selected RS galaxies are shown. Where no RS is detected at the lens redshift, a nominal RS for the lens redshift is shown with a slope of $\beta_V = 0.09$. In many cases, the detected RS is not apparent to the unaided eye, but our spectroscopy has established that these are physical systems, showing the power of our algorithm.

Figure 7 presents sky maps of galaxies in each of the eight detected RSs near z_{lens} . In many cases, the galaxies appear to be clustered, as would be expected in a physical group. In a few cases, such as BRI0952, there appears to be little, if any clustering of galaxies, yet M06 do find a physical group around BRI0952 at the lens redshift.

The sky maps also show that the lens galaxy (indicated by a star at the origin in each plot) is not necessarily at the center of the group. Table 7 presents the raw and luminosity-weighted projected centroids for each candidate RS, plus (where available) the offset between the raw RS centroid and the centroid of spec-

troscopically confirmed group members from M06. For four of the six groups, the centroids agree to within 2σ , while for the other two (MG0751: MWKZ Group 1 and BRI0952: MWKZ Group 1), the photometric and spectroscopic centroids disagree. In these cases, the disagreement could be due to contamination of the photometric sample by non-member galaxies, to incompleteness in the spectroscopic sample, or to some combination of the two. We are analyzing additional spectroscopic data for these groups, which should improve the spectroscopic completeness and hence the centroid accuracy.

Among the eight lenses with an RS at the lens redshift, the lens galaxy position is within 1σ of the projected RS centroid for two systems, and within 3σ for two more. Stated another way, in four cases the lens galaxy is *not* consistent with lying at the centroid (even accounting for the centroid uncertainties). This strongly suggests that lenses do not necessarily occupy the center of the local mass distribution, which is an important realization for lens modeling (see §4.4 and M06).

4.1.2. The Fraction of Lenses with Line-of-Sight Structures

Seven of the twelve lens systems have RSs that are fore or aft of the lens along the line of sight; prior to this study, only one of these groups (B0712) was known to have a line-of-sight group, at $z \approx 0.29$ (Fassnacht & Lubin 2002). This group is not detected here, although we do detect a background group at $z \approx 0.67$. Two of the line-of-sight systems (MG0751: MWKZ Group 2 and RXJ1131: MWKZ Group 1) have very rich RSs indicative of a rich group or even a cluster of galaxies, while the remaining six are more suggestive of poor groups.

Figure 8 shows the CMDs for all candidate line-of-sight groups. We observe a rich, tight RS in RXJ1131, indicative of a foreground cluster of galaxies; indeed, two of these galaxies have redshift measurements of $z \approx 0.10$ from the Las Campanas Redshift Survey (Shectman et al. 1996), and there is extended X-ray emission consistent with their position (C. Kochanek, private communication). Some of the candidate RSs appear dubious, such as the background groups in MG0751 and HE2149. Once again, however, our spectroscopic follow-up confirms the existence of these groups.

Based on the simulations presented in §3.2, we expect

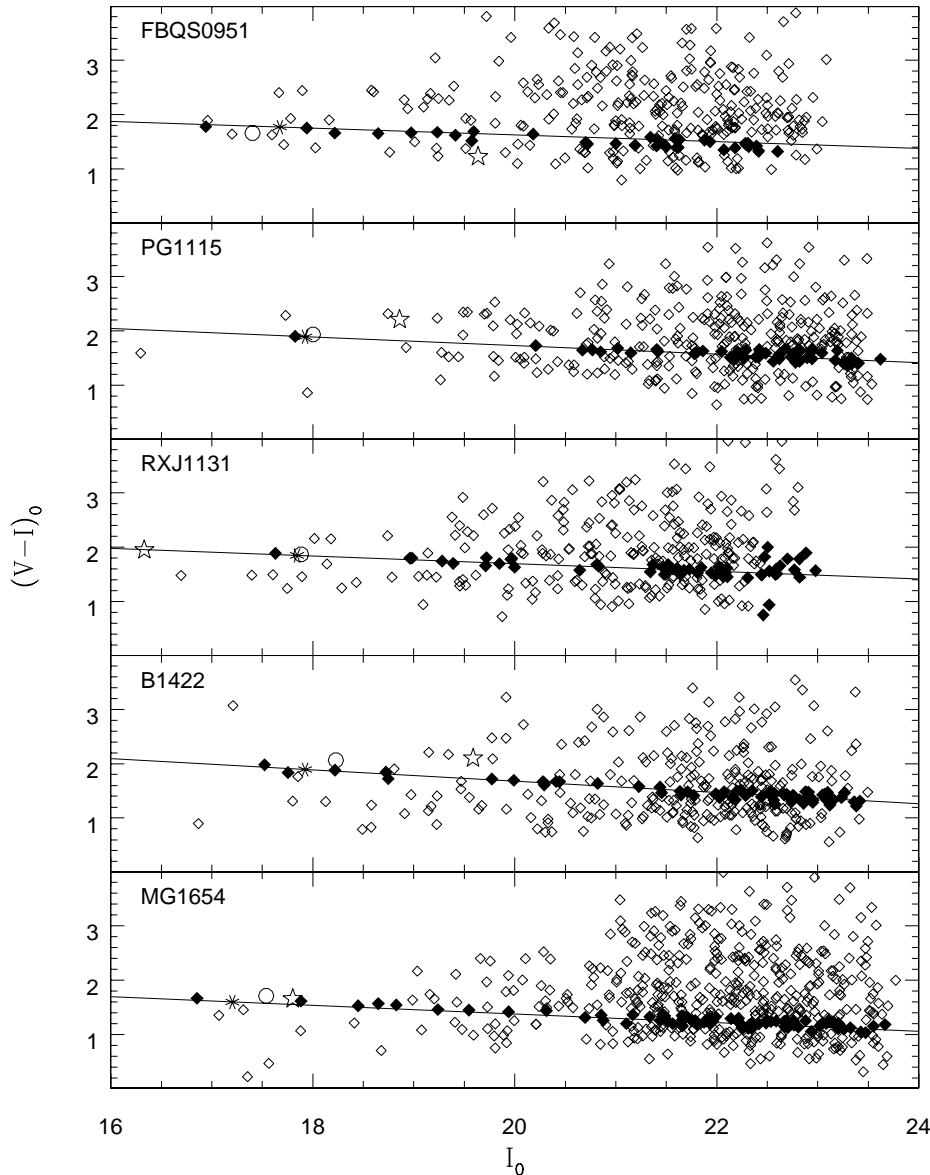


FIG. 6.— Color-magnitude diagrams and red sequences at the lens redshift. Each panel presents an individual lens. Open diamonds show all galaxies within $r_{\text{vir}} (\equiv 500h^{-1} \text{ kpc})$ of the group centroid (or of the lens galaxy for those lenses with no detected red sequence). Selected candidate red sequence galaxies are shown as filled diamonds, along with the best-fitting red sequence for galaxies with $I \leq I_* + 2.5$ (solid line). The lens galaxies are denoted by large, open stars. Asterisks indicate the location of an L_* galaxy along the fit red sequence; open circles show the location of an L_* galaxy at z_{lens} . For the lenses with no detected red sequence (B0712, B1600, HE2149, and PMN2004), a dotted line indicates a nominal red sequence with a slope of 0.09 at z_{lens} . Eight of the twelve lenses have a red sequence at the lens redshift.

about one false positive (either line-of-sight or at z_{lens}) among the five lens fields observed in the V -band and two to three false positives from the seven lens fields with R -band data.

4.2. Lens Galaxy Environments and Shear

It is interesting to consider whether observed lens galaxy environments can explain the external tidal shears required in lens models. Shear is created by an asymmetric distribution of mass around the lens galaxy; a simple way to get that is to have the lens galaxy off-

set from the centroid of the group. Historically, several attempts to compare the shear required by lens models with the distribution of galaxies within $\sim 140 \text{ kpc}$ of the lens have yielded mixed results. In two quadruple-image lenses (PG1115 and B1422), the model shear appears to be consistent with the distribution of galaxies near the lens (Hogg & Blandford 1994; Schechter et al. 1997; Keeton & Kochanek 1997; Kundić et al. 1997a; Kundic et al. 1997b). In contrast, in the Einstein ring MG0751, the shear angle is *not* consistent with the immediate lens environment (Lehár et al. 1997) Also, in a

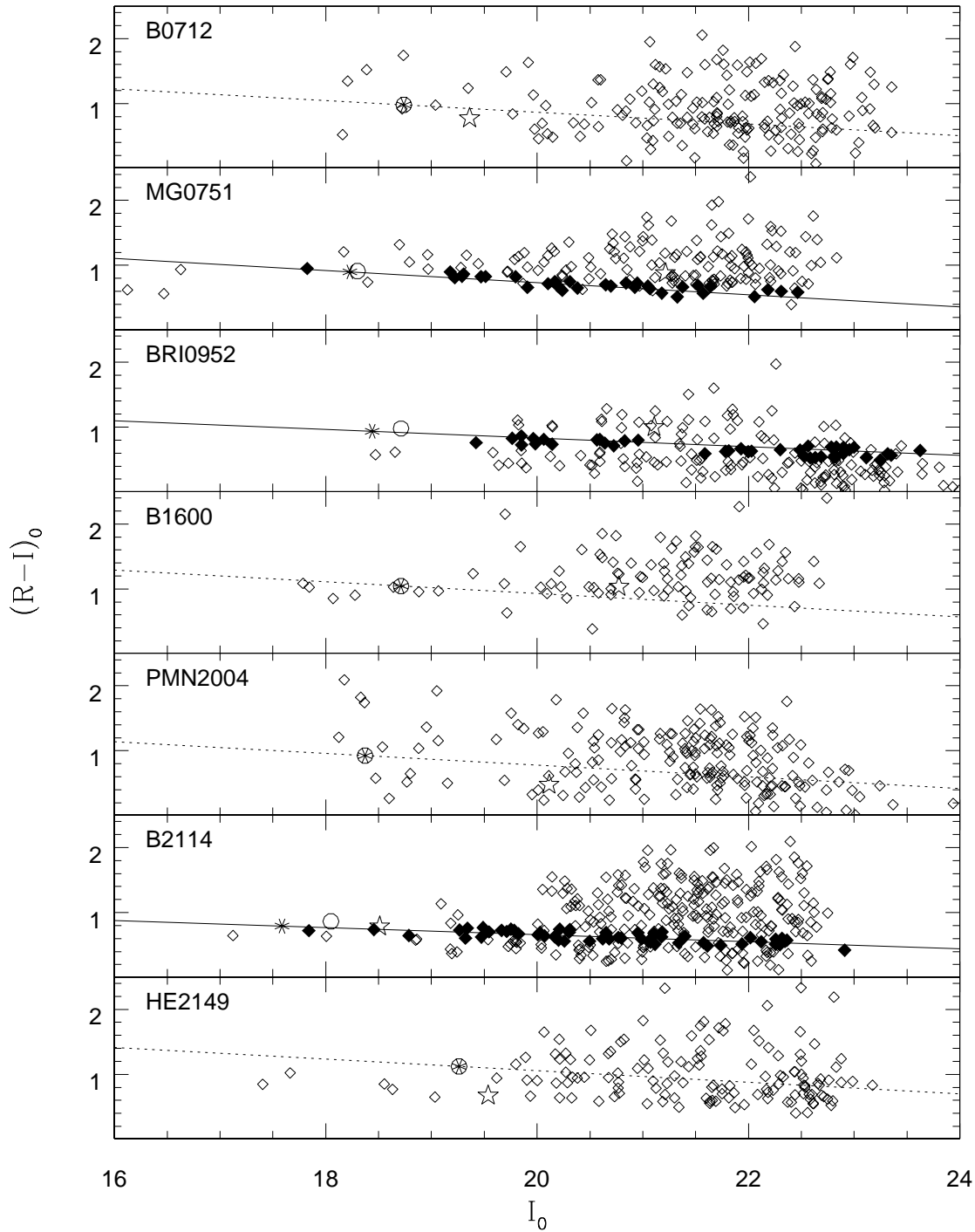


Fig. 6 (cont.)

sample of 10 double-image lenses, Lehár et al. (2000) do not find any strong correlation between model shears and close environments.

We can improve upon the previous studies in three ways. First, we have obtained a larger sample of lens environments. Second, we have measured lens environments over a larger area on the sky. Third, we have

identified enough group member galaxies to make a reliable measurement of the group centroid position. One limitation of our present analysis is that, without measured velocity dispersions, we cannot estimate the amplitude of the shear contributed by each lens environment. (See M06, for an analysis of shear amplitudes for a smaller sample of lenses.) Nevertheless, we can still

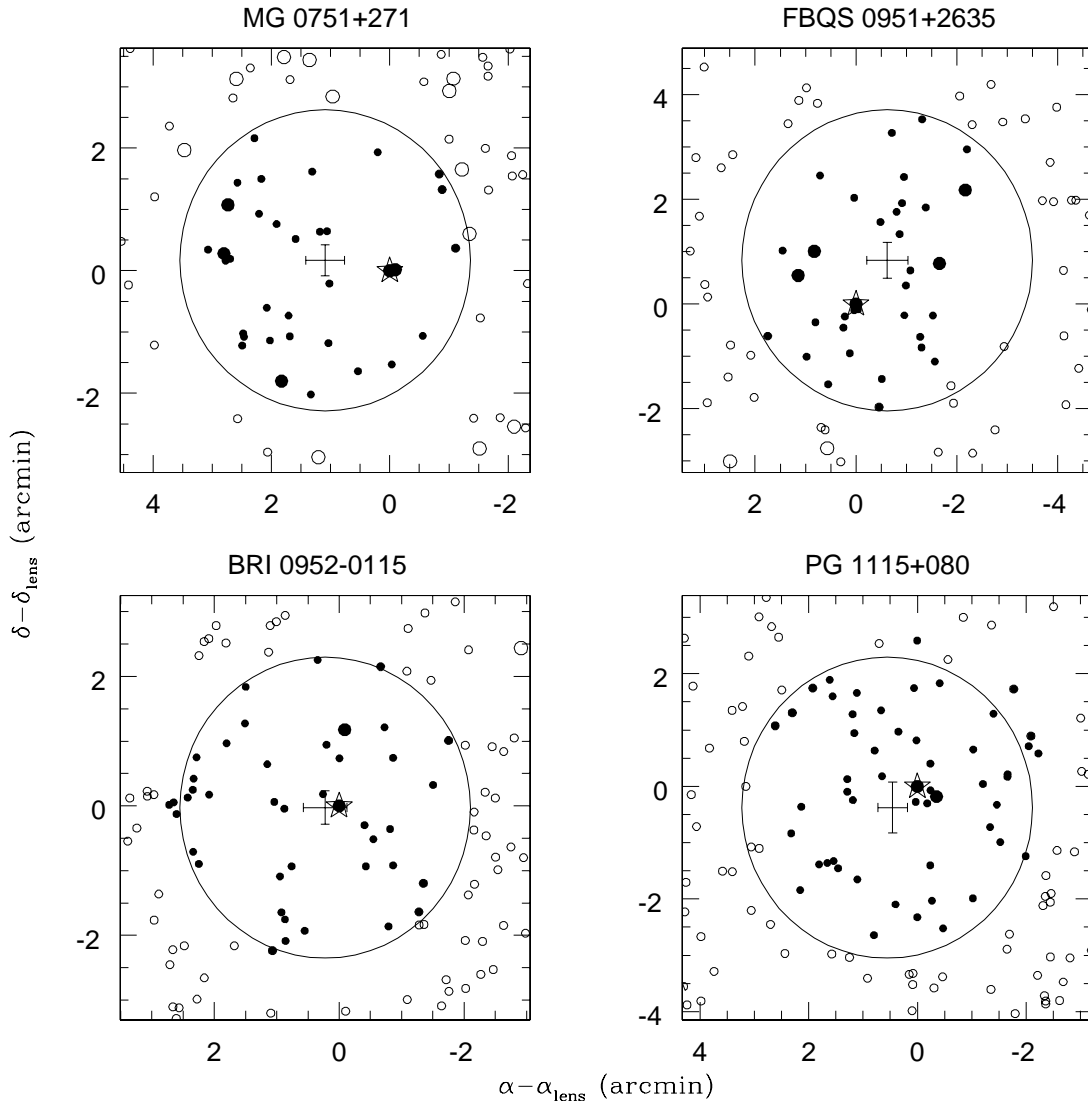


FIG. 7.— Sky maps of red sequence members of candidate lens groups. Point sizes are scaled by galaxy magnitude relative to I_* . The open star at each map’s origin marks the lens position, and the error bars denote the positions of the unweighted red sequence centroids and their 1σ errors. The circle shows one projected group virial radius ($\equiv 500h^{-1}$ kpc) at the red sequence redshift centered on the group centroid. These maps show that, in many cases, the lens galaxy is not consistent with the group centroid and is not the brightest galaxy in the red sequence.

compare the shear position angle with the position angle of the group centroid (relative to the lens galaxy) and determine whether the observed environments are at least consistent with the model shears.

Table 8 gives the position angles for the observed group centroid and the lens model shear, where available. In all six cases where both are available, the centroid and shear position angles are remarkably consistent (albeit with relatively large centroid errorbars in a few cases). Perhaps the most interesting system is MG0751: while the immediate lens environment cannot explain the model shear (Lehár et al. 1997), we now see that the larger environment can. This example illustrates why it is important to observe lens environments over an area large enough to include the full virial extent of a group at the lens redshift. It will be interesting to reconsider this ques-

tion in more detail, after measuring velocity dispersions so that we may estimate shear amplitudes as well as position angles, and after making new lens models of all the systems. Still, it is very encouraging to see new evidence that the observed lens environments can explain the shears required by lens models.

4.3. Lens Galaxy Magnitude Distribution

The sample of lenses allows us to examine the distribution of lens galaxy magnitudes. While bright (i.e., massive) galaxies have large lensing cross-sections, there are many more faint galaxies in groups (e.g., Keeton, Christlein, & Zabludoff 2000). Taken together, these effects lead one to expect the typical lens to be $\sim L_*$ (Kochanek et al. 2000, 2001), though it is still unclear how faint (and dwarf-like) lenses can be. In our sample, *ten* of the eleven lens galaxies with redshift mea-

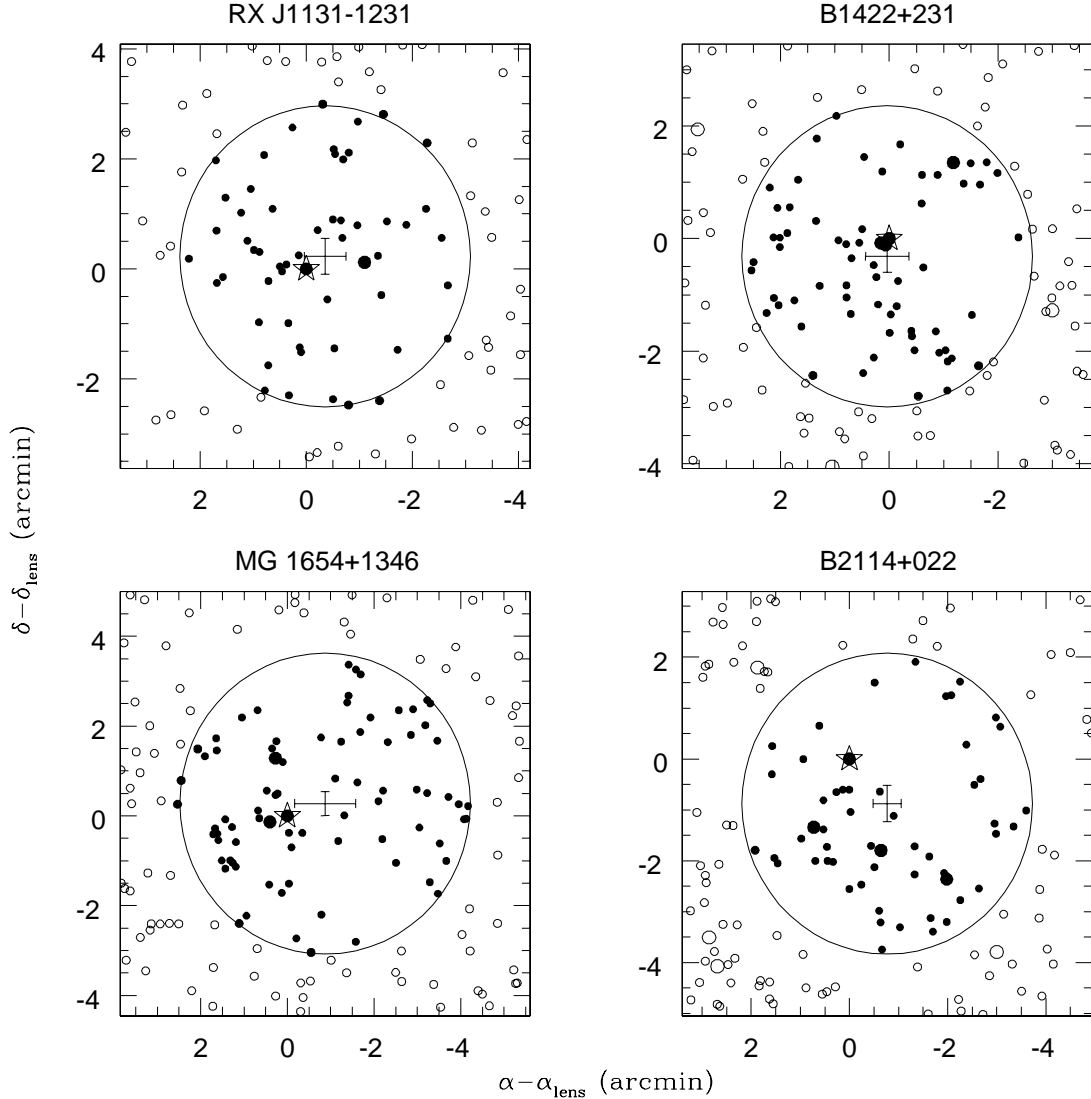


Fig. 7 (cont.)

measurements are fainter than I_* (see Table 9). In order to determine whether our sample includes some unknown bias toward faint lenses (although one would expect that any bias would be toward bright, massive galaxies), we calculate the expected distribution of lens galaxy magnitudes based on theoretical expectations and a minimal number of reasonable assumptions. We then compare this theoretical distribution with the observed distribution in our sample and a larger sample of gravitational lens galaxies from Rusin et al. (2003).

Lensing's sensitivity to mass means that the distribution of lens galaxy magnitudes is not the same as the galaxy luminosity function. Nevertheless, it is straightforward to predict the magnitude distribution for lens galaxies (e.g., Fukugita & Turner 1991). For a singular isothermal sphere lens model, the lensing probability $F \propto \sigma_l^4$, where σ_l is the velocity dispersion of the lensing galaxy (Fukugita & Turner 1991). Assuming a Faber-Jackson relation $L \propto \sigma^{\gamma_{FJ}}$ (Faber & Jackson 1976), we derive a lensing probability $\propto L^{4/\gamma_{FJ}}$.

We begin with a Schechter luminosity function (Schechter 1976),

$$\phi_l(L) dL = \frac{n_*}{L_*} \left(\frac{L}{L_*} \right)^\alpha e^{-L/L_*} dL. \quad (10)$$

Factoring in the lensing probability, the probability for a lens galaxy to have a luminosity L is

$$g_l(L) dL = \frac{n'_*}{L_*} \left(\frac{L}{L_*} \right)^{\alpha+4/\gamma_{FJ}} e^{-L/L_*} dL. \quad (11)$$

We integrate this equation and normalize to a limiting luminosity L_{lim} (thereby accounting for bias due to magnitude-limited surveys and non-converging functions) to get the cumulative probability for lens galaxy luminosities greater than L/L_* ,

$$G_l(L) = \frac{1 - \Gamma(1 + \alpha + 4/\gamma_{FJ}, L/L_*)}{1 - \Gamma(1 + \alpha + 4/\gamma_{FJ}, L_{\text{lim}}/L_*)}, \quad (12)$$

where Γ is the normalized incomplete gamma function. This equation is readily modified to I magnitudes using

TABLE 7
CENTROIDS OF CANDIDATE RED SEQUENCES

RS ID	Raw Centroid		L -weighted Centroid		Offset from M06 ($''$)
	α	δ	α	δ	
B0712: GROUP 1	07 16 03	47 09 25	07 16 03	47 09 14	...
MG0751: GROUP 1	07 51 48	27 16 42	07 51 47	27 16 45	101 ± 20
MG0751: GROUP 2	07 51 44	27 17 10	07 51 44	27 17 09	...
FBQS0951: GROUP 1	09 51 22	26 35 01	09 51 23	26 35 10	...
FBQS0951: GROUP 2	09 51 20	26 36 19	09 51 19	26 36 19	...
FBQS0951: GROUP 3	09 51 22	26 36 01	09 51 23	26 35 51	...
BRI0952: GROUP 1	09 55 03	-01 30 02	09 55 03	-01 30 01	107 ± 41
PG1115: GROUP 3	11 18 16	07 43 27	11 18 16	07 43 12	...
PG1115: GROUP 1	11 18 18	07 45 27	11 18 17	07 45 47	20 ± 22
PG1115: GROUP 2	11 18 18	07 46 03	11 18 19	07 46 24	...
RXJ1131: GROUP 1	11 32 00	-12 31 48	11 32 03	-12 32 03	...
RXJ1131: GROUP 2	11 31 50	-12 31 45	11 31 49	-12 31 45	...
B1422: GROUP 1	14 24 38	22 55 54	14 24 37	22 56 15	40 ± 24
B1600: GROUP 1	16 01 45	43 16 48	16 01 45	43 16 44	...
MG1654: GROUP 1	16 54 37	13 46 38	16 54 40	13 46 39	54 ± 39
B2114: GROUP 1	21 16 47	02 24 54	21 16 47	02 24 41	68 ± 40
HE2149: GROUP 3	21 52 08	-27 32 17	21 52 06	-27 32 09	...
HE2149: GROUP 4	21 52 06	-27 31 31	21 52 05	-27 31 36	...

NOTE. — Units of right ascension are hours, minutes, and seconds, and units of declination are degrees, arcminutes, and arcseconds (J2000.0).

TABLE 8
COMPARISON OF GROUP CENTROIDS TO LENS PROPERTIES

Lens	Raw Centroid		L -weighted Centroid		Offset (kpc)	Position Angle		Shear PA	Reference
	$\Delta\alpha$	$\Delta\delta$	$\Delta\alpha$	$\Delta\delta$		Raw Centroid	L -weighted		
MG0751	90 ± 18	10 ± 15	76 ± 26	13 ± 14	440 ± 90	84 ± 10	80 ± 14	64	(1)
FBQS0951	-37 ± 22	65 ± 20	-53 ± 32	65 ± 16	310 ± 90	-30 ± 17	-39 ± 19
BRI0952	47 ± 21	4 ± 16	48 ± 18	6 ± 18	240 ± 110	85 ± 27	83 ± 24	66	(2)
PG1115	15 ± 16	-32 ± 27	-4 ± 22	-12 ± 20	160 ± 110	155 ± 47	-162 ± 78	-113	(3)
RXJ1131	-21 ± 23	14 ± 20	-35 ± 21	13 ± 15	110 ± 100	-56 ± 58	-70 ± 35	-80	(4)
B1422	2 ± 22	-7 ± 17	-17 ± 18	15 ± 17	30 ± 80	164 ± 86	-49 ± 54	-53	(4)
MG1654	-76 ± 41	16 ± 16	-23 ± 37	17 ± 18	280 ± 140	-78 ± 28	-53 ± 63	-80	(5)
B2114	-58 ± 17	-53 ± 21	-52 ± 18	-66 ± 22	320 ± 80	-132 ± 15	-142 ± 14

REFERENCES. — (1) Lehar et al. 1997, (2) Lehar et al. 2000, (3) Impey et al. 1998, (4) Keeton, Gaudi, & Petters 2003, (5) Kochanek 1995

NOTE. — Units of $\Delta\alpha$ and $\Delta\delta$ are arcseconds (J2000.0). PA measured East of North. Except for PG1115, shear PAs are defined modulo 180 degrees.

TABLE 9
LENS GALAXY MAGNITUDES

Lens	I_{lens}	$I_{0,\text{lens}} - I_*$
B0712	19.58 ± 0.07	0.64
MG0751	21.28 ± 0.64	3.05
FBQS0951	19.68 ± 0.23	2.01
BRI0952	21.23 ± 0.04	2.79
PG1115	18.94 ± 0.02	1.02
RXJ1131	16.6 ± 0.3	-1.3
B1422	19.68 ± 0.25	1.76
B1600	20.80 ± 0.41	1.54
MG1654	17.92 ± 0.02	0.72
PMN2004	20.51 ± 0.02	...
B2114	18.65 ± 0.23	1.06
HE2149	19.60 ± 0.03	0.87

NOTE. — Except for PMN2004, all lens galaxy magnitudes are from the literature (see text).

$L/L_* = 10^{-0.4(I-I_*)}$. Note that Eq. 12 is fully degenerate in α and γ_{FJ} .

We compare two samples to this theoretical prediction. First, we use the nine lenses from the present sample that have early-type lens galaxies (we exclude the two spiral lenses B1600 and PMN2004 and the two-plane lens B2114). Second, we note that as this simple theoretical prediction does not explicitly involve environment, we can also compare it with the larger sample of early-type lens galaxies defined by Rusin et al. (2003), who do not determine the environments of their lenses. The Rusin sample spans a larger redshift range than ours, so we use only the low-redshift systems ($z_{\text{lens}} < 0.6$) with spectroscopic redshifts, a total of 12 lenses. Five of the nine lenses in our sample overlap with the Rusin sample.

We take observed F814W or F791W magnitudes from Rusin et al. (2003) or from the CASTLES web database,⁹ convert to Cousins I , correct for Galactic extinction, and calculate $I - I_*$. For I_* we again use our

⁹ In most cases the lens galaxy magnitude cannot be determined

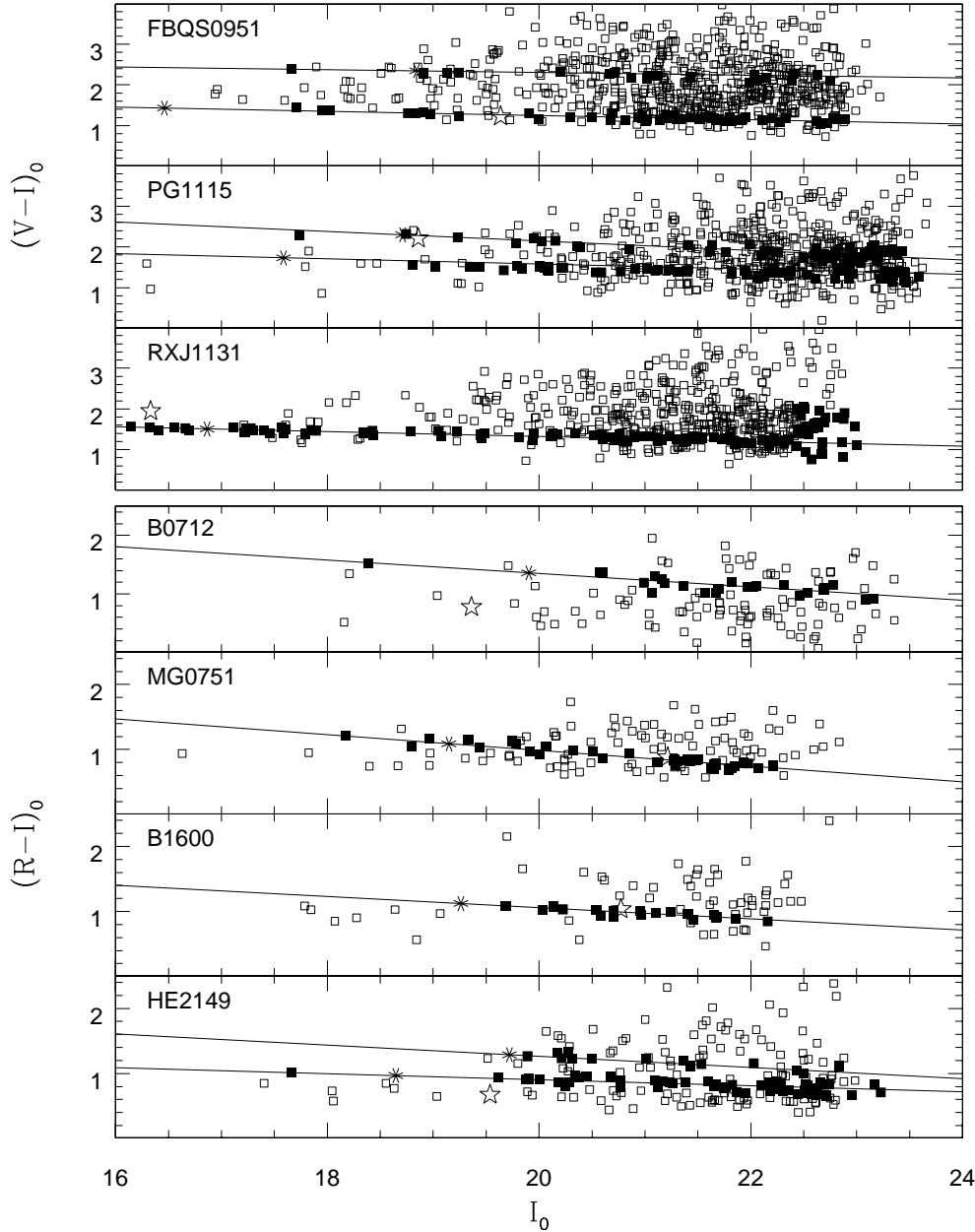


FIG. 8.— Color-magnitude diagrams for candidate line-of-sight red sequences. Symbols are as in Fig. 6. Ten line-of-sight lenses are found in seven (of twelve total) lens fields. Although to the naked eye many of these red sequences are not obvious, our spectroscopic observations of HE2149, MG0751, and PG1115 confirm the line-of-sight groups in HE2149 and MG0751 and the background group in PG1115 (Momcheva et al. 2006). The low- z line-of-sight candidate in PG1115 was not detected spectroscopically. The apparently steeper red-sequence slopes for the lower four panels are due to the smaller vertical color range in $R - I$.

photometric models of early-type galaxies evaluated at the RS photometric redshift (if an RS exists) or at the lens spectroscopic redshift. For our lens sample, we use the photometric RS redshifts to insure consistency with our ongoing, larger lens sample, in which many lens spectroscopic redshifts will not be known. The use of RS photometric redshifts instead of spectroscopic redshifts

from our data, because the lens galaxy and quasar images are unresolved.

does not affect any of our conclusions here.

The cumulative distributions of observed lens galaxy magnitudes are shown in Figure 9, along with predicted distributions for different values of α and γ_{FJ} . Because our sample extends fainter than the Rusin sample ($I_{\text{lim}} - I_* \approx 3$ versus 1.5, respectively), the two observed samples are plotted separately. There is, however, no significant difference between our sample and the Rusin low-redshift subsample: the Kolmogorov-Smirnov (KS)

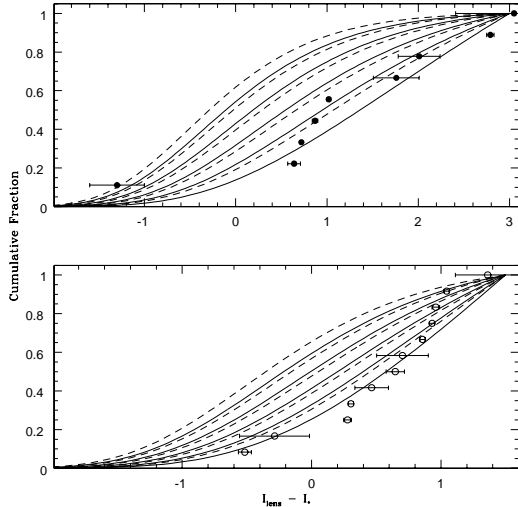


FIG. 9.— Cumulative fraction of lens galaxy magnitudes compared with predicted distributions from Eqn. 12. Solid curves represent $\gamma_{\text{FJ}} = 4$; dashed curves are for $\gamma_{\text{FJ}} = 3.3$, as calculated in Rusin et al. (2003). From left to right, curves are for faint-end luminosity function slopes of $\alpha = -0.6$ to -1.8 in intervals of 0.3, with the middle value of -1.2 shown in bold. Top panel: Lens galaxies in this paper’s sample (solid points), with theoretical curves normalized to $I - I_* = 3$. Bottom panel: $z_{\text{lens}} \leq 0.6$ lens sample of Rusin et al. (2003) (open circles). The lens galaxy magnitude distribution in both samples is well-described by the theoretical models and reasonable values of γ_{FJ} and α .

probability is $P = 0.42$. Both samples indicate that the median low-redshift, early-type lens galaxy has a magnitude $I - I_* \approx 0.75$, or a luminosity $L \approx 0.5L_*$. This median value is directly dependent on the value of I_* ; as discussed in Appendix A, our normalization of I_* is brighter by ~ 1 magnitude than most modern surveys, so the median lens luminosity may well be closer to L_* . Even allowing for this, fully half of the elliptical lens galaxies are fainter than L_* , some significantly so (in particular, BRI0952 and MG0751 are 2 to 3 magnitudes fainter than I_* , having $L \sim 0.1L_*$).

The figure shows that there are values of $\alpha + 4/\gamma_{\text{FJ}}$ leading to theoretical predictions that match the data reasonably well. High values of $\alpha + 4/\gamma_{\text{FJ}}$ are clearly inconsistent with the data: KS tests rule out $\alpha + 4/\gamma_{\text{FJ}} \gtrsim -0.2$ at the 2σ level ($P \leq 0.05$). For reasonable Faber-Jackson slopes ($\gamma_{\text{FJ}} \sim 3$ to 4), this would suggest that the faint-end luminosity function slope is steep, $\alpha \lesssim -1.2$. We note that any selection bias against small image separation lenses will tend to lessen the slope of the observed distribution in Figure 9, as such a bias will be more pronounced in the less massive (and, by assumption, fainter) lenses. This potential bias, the degeneracy between α and γ_{FJ} , and the uncertainty in the normalization in I_* prevent us from drawing detailed conclusions here.

There are several important results from this exercise. On the observational side, the median lens galaxy luminosity is near or below L_* , and the luminosity distribution is very broad. In other words, lens galaxies are not all massive, super- L_* ellipticals; rather, they span a range of luminosities (and, presumably, masses), extending down at least to $\sim 0.1L_*$. On the theoretical side, the observed luminosity distribution is consistent

with simple models of a Schechter luminosity function weighted by the lensing probability, for reasonable values of α and γ_{FJ} . The key conceptual point is that, while lensing selects galaxies by mass, dwarf galaxies are sufficiently common to comprise a moderate fraction of the lens galaxy sample.

4.4. Properties of the Brightest Red Sequence Galaxies

In the local universe, X-ray luminous groups of galaxies with $\sigma \gtrsim 300 \text{ km s}^{-1}$ contain a giant elliptical, the *Brightest Group Galaxy* or BGG (Mulchaey & Zabludoff 1998), which occupies a unique position in the kinematic and projected spatial center of the group (Zabludoff & Mulchaey 1998; van den Bosch et al. 2005). In this section we examine the BGGs in our group sample in order to determine whether any evolution in their properties can be observed. In two of three distant, high- σ ($\sim 300\text{--}500 \text{ km s}^{-1}$) groups, M06 found that the lack of a significant offset of the BGG from the group centroid is similar to that observed in nearby groups. Given the larger sample offered by this photometric study, we identify the BGG in each candidate group and examine its relation to the group centroid. As BGGs at low redshift are typically ellipticals, we assume here that the brightest galaxy on the selected RS (BRSG, for brightest red sequence galaxy) is the BGG.

The properties of the BRSG in each group are given in Table 10. Only two lens galaxies, RXJ1131 and MG1654, are BRSGs. We also note that two BRSGs, those in B2114 Group 1 and HE2149 Group 4, are known not to be the BGG as their redshifts are inconsistent with group membership. The fraction of lens galaxies that are BRSGs is 0.25 (two lenses out of eight lens groups); M06 find a BGG fraction of 0.33 (two lenses out of six lens groups). These values compare favorably with the suggestion by Oguri (2006) than $\lesssim 50\%$ of lens galaxies occupy the dominant halo, the remainder being “satellite” galaxies, or sub-halos within the overall group halo. This result is also not surprising in light of our conclusion in §4.3 that the lens galaxy is typically not a very luminous galaxy.

Figure 10 compares the offset of each BRSG from the raw projected spatial RS centroid to the measured group velocity dispersion from M06. With one exception (MG0751), groups with $\sigma \gtrsim 300 \text{ km s}^{-1}$ have a BRSG near the group centroid, while none of the smaller- σ groups have a central BRSG. A Spearman rank correlation of σ and the centroid-BRSG offset also suggests a trend (the probability of no correlation is 0.14). Our data therefore intimate that there are dynamically evolved (i.e., virialized) groups with high σ and a central, dominant early-type member by $z \sim 0.5$, groups whose properties are consistent with evolved (virialized) groups in the nearby Universe.

4.5. The Ratio of Quad to Double Lenses

One unsolved puzzle in lensing studies is why there are so many quadruple-image lenses compared with double-image lenses (King et al. 1996; Kochanek 1996b; Keeton & Kochanek 1997; Rusin & Tegmark 2001; Cohn & Kochanek 2004; Keeton & Zabludoff 2004). Highly-flattened lens galaxies are one way to obtain

TABLE 10
PROPERTIES OF BRIGHTEST RED SEQUENCE GALAXIES

RS ID	ID _{BRS} G	$I_{0,\text{BRS}G}$	Offset from lens		Offset from centroid		ID _{BGG} ^a	Notes
			(")	(kpc)	(")	(kpc)		
B0712: GROUP 1	8471	18.387	28 ± 10	190 ± 70	...	
MG0751: GROUP 1	8626	17.824	6	30	96 ± 18	460 ± 90	8626	a.k.a. G1 (Tonry & Kochanek 1999)
MG0751: GROUP 2	8387	18.171	34 ± 12	200 ± 70	8476	Brighter than M06 BGG
FBQS0951: GROUP 1	7859	17.713	128 ± 49	350 ± 130	...	
FBQS0951: GROUP 2	9345	16.941	110	450	65 ± 22	270 ± 90	...	
FBQS0951: GROUP 3	8679	17.665	18 ± 20	100 ± 110	...	
BRI0952: GROUP 1	9622	19.422	71	360	84 ± 18	430 ± 90	8406	Brighter than M06 BGG
PG1115: GROUP 3	11679	18.804	106 ± 21	430 ± 90	...	
PG1115: GROUP 1	12600	17.824	24	110	42 ± 19	190 ± 90	12600	a.k.a. G1 (Impey et al. 1998)
PG1115: GROUP 2	13804	17.732	101 ± 17	550 ± 90	13764	Brighter than M06 BGG
RXJ1131: GROUP 1	7236	15.135	44 ± 22	140 ± 70	...	$z = 0.104$ from LCRS
RXJ1131: GROUP 2	6323	16.6	0	0	25 ± 22	110 ± 100	...	Lens galaxy
B1422: GROUP 1	13152	17.523	8	40	2 ± 22	10 ± 100	13152	
B1600: GROUP 1	7950	19.714	88 ± 15	540 ± 90	...	
MG1654: GROUP 1	17334	17.92	0	0	78 ± 40	280 ± 140	17334	Lens galaxy
B2114: GROUP 1	7943	17.841	185	740	108 ± 20	430 ± 80	8938	Not group member (M06)
HE2149: GROUP 3	7568	17.663	80 ± 15	430 ± 80	8364	Brighter than M06 BGG
HE2149: GROUP 4	7534	19.892	54 ± 16	360 ± 110	6342	Not group member (M06)

^aID of BGG in M06

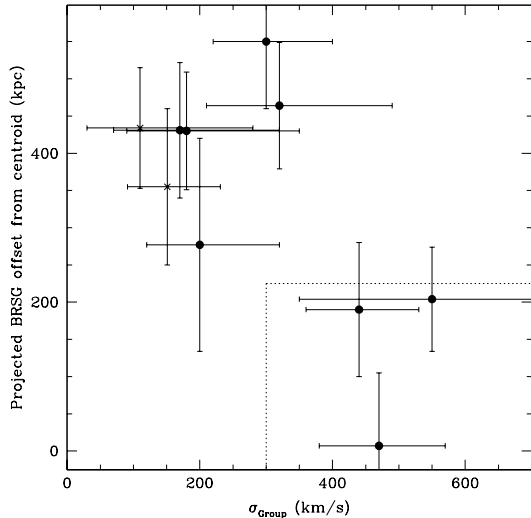


FIG. 10.— Offset of the brightest red-sequence galaxy (BRS) from the red sequence centroid as a function of spectroscopic group velocity dispersion (from M06). Crosses represent BRSs known not to be the brightest group galaxy (see Table 10). The dotted box indicates the maximum spatial offset of BGGs in groups with $\sigma_{\text{group}} > 300 \text{ km s}^{-1}$ in the local Universe (Zabludoff & Mulchaey 1998). As in the local Universe, higher velocity dispersion groups have a BGG near the group centroid, while lower velocity dispersion groups do not.

the seemingly high numbers of quad lenses; another possibility is the presence of a large tidal shear from mass near the lens galaxy or along the line-of-sight. In this latter scenario, quad lenses might be expected to be located preferentially in complex environments or along cluttered lines of sight. Indeed, M06 note that in a sample of eight lenses, both of the quad lenses and the one quad/ring lens are in relatively massive groups, while another ring and two of the doubles are in poorer groups, and the other two doubles have no

groups around the lens galaxies.

Photometrically, we find some weak evidence that quad lenses may have more complex environments than double lenses. Three of the four quad lenses and all three “other” lenses have associated RSs, while only two of the five double-image lenses have RSs. However, this difference is not statistically significant; larger samples are needed to make any definitive statement. The lack of strong evidence for a difference between quad and double lens environments contrasts with our findings in M06. The difference may simply reflect small number statistics. A more likely explanation is that the results in M06 were based on detailed calculations of the convergence and shear due to each lens environment — calculations we cannot make in this paper because we do not know the true memberships and velocity dispersions for all of our groups. Our complete lens sample will enable us to reexamine any connections between image number and environment that may be hidden in the noise of our current sample.

We find no correlation between the number of lensed images and the presence/absence of line-of-sight structures. Three of the four quads, three of the five doubles, and two of the three “others” have at least one line-of-sight structure identified photometrically. Again we need more data to draw a strong conclusion about any possible relation.

5. CONCLUSIONS

We have presented the first results from an ongoing wide-field imaging survey of ~ 80 strong gravitational lens systems. We use a modified version of the Gladders & Yee (2000) group-finding algorithm to locate potential red sequences, both at the lens redshift and along the line-of-sight, in the fields of twelve lenses. This modified algorithm is capable of detecting $\sigma \gtrsim 200 - 300 \text{ km s}^{-1}$ poor groups out to $z \approx 0.4$, and higher- σ groups out to higher redshifts with a low rate of false positives and reasonable completeness.

We draw the following conclusions:

- Most gravitational lenses lie in complex environments. For this sample, 67% of lens galaxies (eight of twelve) lie in galaxy groups. As there are no strong biases in this sample, it is unlikely this fraction would drop below $\sim 50\%$ once the environments of all lenses are surveyed.
- Most gravitational lenses have interloping structures. In particular, we detect ten groups projected within ~ 1.5 of seven lenses; i.e., $\approx 60\%$ of the lenses in this sample have at least one interloping group that could impact the lens model (see also Momcheva et al. 2006).
- The centroid positions of the lens groups are consistent with the directions of the external shears required by lens models, for the six systems where we can make the comparison. This suggests that lens environments can explain the model shears — which has often been assumed, but not well proven. In at least one system (MG0751), the agreement is seen only when the full virial extent of the group is included.
- The typical gravitational lens is not a super- L_* elliptical. Rather, the observed distribution of lens magnitudes is well-described by a convolution of lensing probabilities with a Schechter (1976) luminosity function, with a median lens galaxy luminosity $\sim L_*$ and with known lens galaxies as faint as $\sim 0.1L_*$.
- The typical lens galaxy is not the brightest group galaxy. In the current sample, only two of eight lens galaxies (25%) in a group are the brightest group galaxy.
- As in the local Universe, higher velocity dispersion ($\sigma \gtrsim 300 \text{ km s}^{-1}$), intermediate-redshift galaxy groups have a brightest group galaxy near the group centroid, whereas the brightest group galaxy typically lies outside the group center in lower velocity dispersion groups. This result suggests that the higher σ groups are more dynamically evolved (i.e., virialized) than the lower- σ groups and that evolved (virialized) groups exist by $z \sim 0.5$.
- In total, we report the photometric discovery or recovery of 18 candidate poor groups of galaxies

in the redshift range $z \sim 0.2$ to 0.6 . The average red sequence slope is 0.076 ± 0.025 , in agreement with that of nearby groups. The measured scatter about the red sequence is comparable to that expected from random photometric errors. When analysis of the full lens sample is complete, we expect to find ~ 100 groups at these intermediate redshifts, permitting detailed studies of the evolution of group structure and members.

The authors are grateful for support for this project in the form of National Science Foundation grant AST-0206084 and NASA LTSA award NAGS-11108. CRK was supported in part by NASA through Hubble Fellowship grant HST-HF-01141.01-A from the Space Telescope Science Institute, which is operated by the Association of Universities for Research in Astronomy, Inc., under NASA contract NAS5-26555. IM acknowledges the support of the Martin F. McCarthy Scholarship in Astrophysics awarded by the Vatican Observatory.

We thank Dennis Zaritsky, Greg Rudnick, Luc Simard, and Chien Peng for helpful discussions along the way. We thank the referee, Chris Kochanek, for comments that improved this paper. We also thank Mike Brown (the Aussie) and Doug Clowe for snippets of software used in the analysis. We especially thank Emilio Falco for his vital assistance in the formulating the initial target lists.

Observations were made at Kitt Peak National Observatory and the Cerro-Tololo Inter-American Observatory, as part of the National Optical Astronomy Observatory, which is operated by the Association of Universities for Research in Astronomy, Inc. (AURA) under cooperative agreement with the National Science Foundation. The authors also would like to express their appreciation to the excellent staff at both of these facilities, especially to the excellent telescope operators and the computer support staff who saved many gigabytes of data on more than one occasion.

The authors wish to recognize and acknowledge the significant cultural role and reverence that Kitt Peak holds within the Native American community, in particular the Tohono O’odham Nation. We are most fortunate to have the opportunity to conduct observations from this mountain.

APPENDIX

PREDICTED GALAXY PHOTOMETRIC PROPERTIES

For this paper, we determine the photometric properties of galaxies as a function of redshift from simple evolutionary models already used for analysis of lens galaxies (Keeton et al. 1998). These models begin with spectrophotometric models by Bruzual & Charlot (1993), assuming solar metallicity and a star formation epoch starting at $z = 5$. We assume that early-type galaxies are formed by a 1-Gyr burst of star formation with a Salpeter (1955) initial mass function (IMF) followed by passive evolution to the present day. We model late-type galaxies with a Scalo (1986) IMF and with the star formation rates from Guiderdoni & Rocca-Volmerange (1988) for Sa, Sb, and Sc galaxies. We use these models to compute the color-, K -, and evolutionary corrections needed to predict the apparent magnitude and colors of an L_* galaxy as a function of redshift. For this work, we define L_* to be the luminosity of a $z = 0$ galaxy with an absolute B -band magnitude of $M_B(L_*) = -19.9 + 5 \log h$. The model color-magnitude curves are shown in Figure 11.

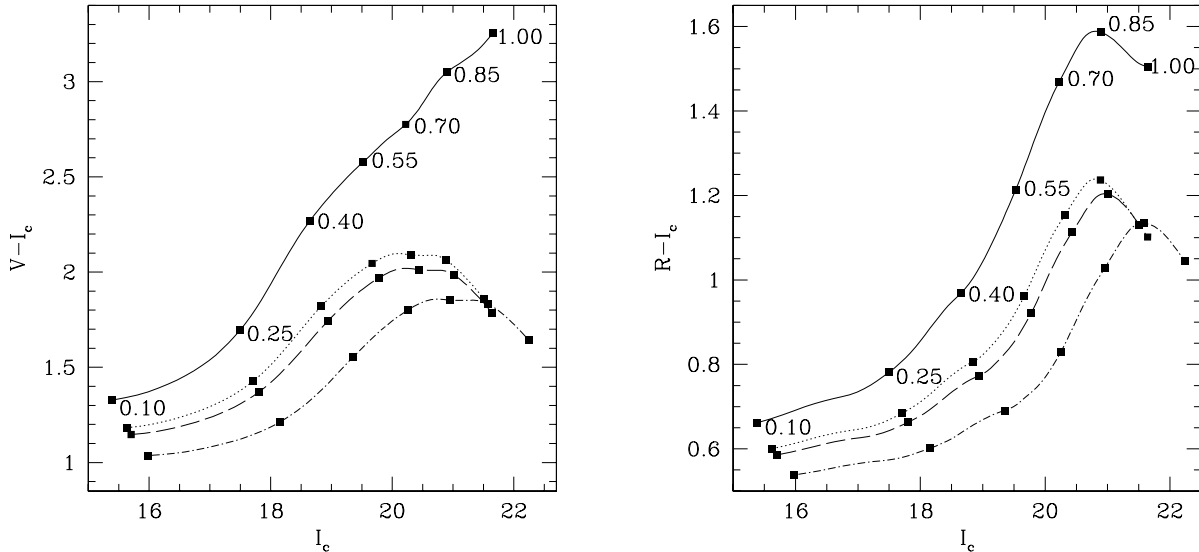


FIG. 11.— Model galaxy $V - I$ (left) and $R - I$ (right) colors versus I magnitude for an L_* galaxy. Curves indicate E/S0 (solid), Sa (dotted), Sb (dashed), and Sc (dot-dashed) galaxies and range from $z = 0.1 - 1.0$. Boxes mark redshift intervals of $\Delta z = 0.15$, with the corresponding numerical redshift indicated along the E/S0 track.

We also consider the impact of different normalizations of $M_B(L_*)$ on our results. We have converted each of the published normalizations to a consistent cosmology and to M_B , the latter by using the $z = 0$ colors for elliptical galaxies calculated by Fukugita, Shimasaku, & Ichikawa (1995). Recent analysis of the density-dependence of the galaxy luminosity function from the 2dF Galaxy Redshift Survey (Colless et al. 2001) is presented in Croton et al. (2005), who find $M_B(L_*)$ ranging from $-18.3 + 5 \log h$ for early-type galaxies in voids to $-19.8 + 5 \log h$ for early-type galaxies in clusters, with a value $\approx -19.4 + 5 \log h$ for the entire volume. Bernardi et al. (2005) find a value of $M_B(L_*) = -18.9 + 5 \log h$ for early-type galaxies from the Sloan Digital Sky Survey. Other galaxy surveys have values of $M_B(L_*)$ ranging from $\approx -18.7 + 5 \log h$ to $\approx -19.4 + 5 \log h$ (e.g., see Table 1 in Gonzalez et al. 2000).

Analytically, the change in the color $V - I$ of a galaxy of magnitude I on the red sequence from a change in normalization of I_* of ΔI_* is:

$$\Delta(V - I) = \beta_V \Delta I_*, \quad (\text{A1})$$

where β_V is the slope of the red sequence in $V - I$. Taking the faintest value of $M_B(L_*) = -18.3 + 5 \log h$ from the surveys above and $\beta_V = 0.08$ (§3.1), the maximum change in the color of a red sequence galaxy is $\Delta(V - I) = -0.128$. Over the redshift range of $0.2 < z < 1.0$, the average change in photometric redshift as a function of change in color is $\Delta z / \Delta(V - I) = 0.133$, so the maximum change in redshift from a change in normalization would be $\Delta z \approx -0.02$. We test this calculation by running the group-finding algorithm on several groups with $M_B(L_*) = -18.3 + 5 \log h$, and indeed the detected group redshifts are lower by ≈ 0.02 . We therefore note that our photometric group redshifts may be systematically biased toward higher redshifts by as much as $\Delta z = 0.02$, smaller than the measured scatter between groups photometric and spectroscopic redshifts given in §3.3.

REFERENCES

- Abajas, C., Mediavilla, E., Muñoz, J. A., Popović, L. Č., & Oscoz, A. 2002, *ApJ*, 576, 640
 Abazajian, K., et al. 2005, *AJ*, 129, 1755
 Augusto, P., et al. 2001, *MNRAS*, 326, 1007
 Bar-Kana, R. 1996, *ApJ*, 468, 17
 Bell, E. F., et al. 2004, *ApJ*, 608, 752
 Bernardi, M., Sheth, R. K., Nichol, R. C., Schneider, D. P., & Brinkmann, J. 2005, *AJ*, 129, 61
 Bertin, E., & Arnouts, S. 1996, *A&AS*, 117, 393
 Blandford, R. D., & Narayan, R. 1992, *ARA&A*, 30, 311
 Bower, R. G., Lucey, J. R., & Ellis, R. S. 1992, *MNRAS*, 254, 601
 Bruzual A., G., & Charlot, S. 1993, *ApJ*, 405, 538
 Burud, I., et al. 2002, *A&A*, 383, 71
 Carlberg, R. G., Yee, H. K. C., Morris, S. L., Lin, H., Hall, P. B., Patton, D. R., Sawicki, M., & Shepherd, C. W. 2001, *ApJ*, 552, 427
 Chae, K.-H. 2003, *MNRAS*, 346, 746
 Cohn, J. D., & Kochanek, C. S. 2004, *ApJ*, 608, 25
 Coleman, G. D., Wu, C.-C., & Weedman, D. W. 1980, *ApJS*, 43, 393
 Colless, M., et al. 2001, *MNRAS*, 328, 1039
 Cooray, A. R., & Huterer, D. 1999, *ApJ*, 513, L95
 Courbin, F., Saha, P., & Schechter, P. L. 2002, *LNP Vol. 608: Gravitational Lensing: An Astrophysical Tool*, 608, 1
 Croton, D. J., et al. 2005, *MNRAS*, 356, 1155
 Dalal, N., & Kochanek, C. S. 2002, *ApJ*, 572, 25
 Dai, X., & Kochanek, C. S. 2005, *ApJ*, 625, 633
 Faber, S. M., & Jackson, R. E. 1976, *ApJ*, 204, 668
 Fassnacht, C. D., & Cohen, J. G. 1998, *AJ*, 115, 377
 Fassnacht, C. D., & Lubin, L. M. 2002, *AJ*, 123, 627
 Fassnacht, C. D., Gal, R. R., Lubin, L. M., McKean, J. P., Squires, G. K., & Readhead, A. C. S. 2006, *ApJ*, in press (astro-ph/0510728)
 Faure, C., Alloin, D., Kneib, J. P., & Courbin, F. 2004, *A&A*, 428, 741
 Fischer, P., Schade, D., & Barrientos, L. F. 1998, *ApJ*, 503, L127
 Fukugita, M., & Turner, E. L. 1991, *MNRAS*, 253, 99
 Fukugita, M., Shimasaku, K., & Ichikawa, T. 1995, *PASP*, 107, 945
 Gerke, B. F., et al. 2005, *ApJ*, 625, 6
 Gladders, M. D., & Yee, H. K. C. 2000, *AJ*, 120, 2148

- Gonzalez, A. H., Williams, K. A., Bullock, J. S., Kolatt, T. S., & Primack, J. R. 2000, *ApJ*, 528, 145
- Gonzalez, A. H., Zaritsky, D., Dalcanton, J. J., & Nelson, A. 2001, *ApJS*, 137, 117
- Grant, C. E., Bautz, M. W., Chartas, G., & Garmire, G. P. 2004, *ApJ*, 610, 686
- Guiderdoni, B., & Rocca-Volmerange, B. 1988, *A&AS*, 74, 185
- Hogg, D. W., & Blandford, R. D. 1994, *MNRAS*, 268, 889
- Impey, C. D., Falco, E. E., Kochanek, C. S., Lehár, J., McLeod, B. A., Rix, H.-W., Peng, C. Y., & Keeton, C. R. 1998, *ApJ*, 509, 551
- Jackson, N., et al. 1995, *MNRAS*, 274, L25
- Jackson, N., et al. 1998, *MNRAS*, 296, 483
- Keeton, C. R., & Kochanek, C. S. 1997, *ApJ*, 487, 42
- Keeton, C. R., Kochanek, C. S., & Seljak, U. 1997, *ApJ*, 482, 604
- Keeton, C. R., Kochanek, C. S., & Falco, E. E. 1998, *ApJ*, 509, 561
- Keeton, C. R., Christlein, D., & Zabludoff, A. I. 2000, *ApJ*, 545, 129
- Keeton, C. R., Gaudi, B. S., & Petters, A. O. 2003, *ApJ*, 598, 138
- Keeton, C. R., & Zabludoff, A. I. 2004, *ApJ*, 612, 660
- King, L. J., & Browne, I. W. A. 1996, *MNRAS*, 282, 67
- King, L. J., Browne, I. W. A., & Wilkinson, P. N. 1996, *IAU Symp. 173: Astrophysical Applications of Gravitational Lensing*, 173, 191
- Kneib, J.-P., Cohen, J. G., & Hjorth, J. 2000, *ApJ*, 544, L35
- Kochanek, C. S. 1991, *ApJ*, 373, 354
- Kochanek, C. S. 1995, *ApJ*, 445, 559
- Kochanek, C. S. 1996a, *ApJ*, 466, 638
- Kochanek, C. S. 1996b, *ApJ*, 473, 595
- Kochanek, C. S., et al. 2000, *ApJ*, 543, 131
- Kochanek, C. S., et al. 2001, *ASP Conf. Ser. 237: Gravitational Lensing: Recent Progress and Future Goals*, 237, 159
- Kochanek, C. S., White, M., Huchra, J., Macri, L., Jarrett, T. H., Schneider, S. E., & Mader, J. 2003, *ApJ*, 585, 161
- Kochanek, C. S. 2004, *ApJ*, 605, 58
- Kochanek, C. S., & Schechter, P. L. 2004, *Measuring and Modeling the Universe*, 117
- Kormendy, J. 1977, *ApJ*, 218, 333
- Kron, R. G. 1980, *ApJS*, 43, 305
- Kundić, T., Cohen, J. G., Blandford, R. D., & Lubin, L. M. 1997, *AJ*, 114, 507
- Kundic, T., Hogg, D. W., Blandford, R. D., Cohen, J. G., Lubin, L. M., & Larkin, J. E. 1997, *AJ*, 114, 2276
- La Barbera, F., Busarello, G., Merluzzi, P., Massarotti, M., & Capaccioli, M. 2003, *ApJ*, 595, 127
- Landolt, A. U. 1992, *AJ*, 104, 340
- Langston, G. I., et al. 1989, *AJ*, 97, 1283
- Lehár, J., et al. 1997, *AJ*, 114, 48
- Lehár, J., et al. 2000, *ApJ*, 536, 584
- Lewis, G. F., & Ibata, R. A. 2004, *MNRAS*, 348, 24
- Lin, H., Yee, H. K. C., Carlberg, R. G., Morris, S. L., Sawicki, M., Patton, D. R., Wirth, G., & Shepherd, C. W. 1999, *ApJ*, 518, 533
- Lopez, S., Wucknitz, O., & Wisotzki, L. 1998, *A&A*, 339, L13
- Mao, S., & Schneider, P. 1998, *MNRAS*, 295, 587
- Massey, P., et al. 2002, "A Direct Imaging Manual for Kitt Peak," <http://www.noao.edu/kpno/manuals/dim/dim.html>
- McIntosh, D. H., Zabludoff, A. I., Rix, H., & Caldwell, N. 2005, *ApJ*, 619, 193
- McMahon, R., & Irwin, M. 1992, *GEMINI Newsletter Royal Greenwich Observatory*, 36, 1
- Metcalfe, R. B., & Madau, P. 2001, *ApJ*, 563, 9
- Metcalfe, R. B., Moustakas, L. A., Bunker, A. J., & Parry, I. R. 2004, *ApJ*, 607, 43
- Miles, T. A., Raychaudhury, S., Forbes, D. A., Goudfrooij, P., Ponman, T. J., & Kozhurina-Platais, V. 2004, *MNRAS*, 355, 785
- Mitchell, J. L., Keeton, C. R., Frieman, J. A., & Sheth, R. K. 2005, *ApJ*, 622, 81
- Momcheva, I., Williams, K. A., Zabludoff, A. I., & Keeton, C. R. 2006, *ApJ*, 641, 169
- Mulchaey, J. S., & Zabludoff, A. I. 1998, *ApJ*, 496, 73
- Oguri, M., 2005, *MNRAS*, in press (astro-ph/0508528)
- Patnaik, A. R., Browne, I. W. A., Walsh, D., Chaffee, F. H., & Foltz, C. B. 1992, *MNRAS*, 259, 1P
- Premadi, P., & Martel, H. 2004, *ApJ*, 611, 1
- Rauch, K. P., & Blandford, R. D. 1991, *ApJ*, 381, 39
- Refsdal, S. 1964, *MNRAS*, 128, 307
- Richards, G. T., et al. 2004, *ApJ*, 610, 679
- Rieke, G. H., & Lebofsky, M. J. 1985, *ApJ*, 288, 618
- Roberts, D. H., Lehar, J., Hewitt, J. N., & Burke, B. F. 1991, *Nature*, 352, 43
- Rusin, D., & Tegmark, M. 2001, *ApJ*, 553, 709
- Rusin, D., et al. 2003, *ApJ*, 587, 143
- Rusin, D., & Kochanek, C. S., 2005, *ApJ*, 623, 666
- Salpeter, E. E. 1955, *ApJ*, 121, 161
- Scalo, J. M. 1986, *Fundamentals of Cosmic Physics*, 11, 1
- Schechter, P. 1976, *ApJ*, 203, 297
- Schechter, P. L., et al. 1997, *ApJ*, 475, L85
- Schechter, P. L., Gregg, M. D., Becker, R. H., Helfand, D. J., & White, R. L. 1998, *AJ*, 115, 137
- Schechter, P. L. 2005, *IAU Symposium*, 225, 281
- Schlegel, D. J., Finkbeiner, D. P., & Davis, M. 1998, *ApJ*, 500, 525
- Seljak, U. 1994, *ApJ*, 436, 509
- Shetman, S. A., Landy, S. D., Oemler, A., Tucker, D. L., Lin, H., Kirshner, R. P., & Schechter, P. L. 1996, *ApJ*, 470, 172
- Simard, L., et al. 2002, *ApJS*, 142, 1
- Sluse, D., et al. 2003, *A&A*, 406, L43
- Smith, J. A., et al. 2002, *AJ*, 123, 2121
- Stetson, P. B. 1987, *PASP*, 99, 191
- Tonry, J. L. 1998, *AJ*, 115, 1
- Tonry, J. L., & Kochanek, C. S. 1999, *AJ*, 117, 2034
- Tonry, J. L., & Kochanek, C. S. 2000, *AJ*, 119, 1078
- Treu, T., & Koopmans, L. V. E. 2002a, *ApJ*, 575, 87
- Treu, T., & Koopmans, L. V. E. 2002b, *MNRAS*, 337, 6
- Turner, E. L. 1990, *ApJ*, 365, L43
- van den Bosch, F. C., Weinmann, S. M., Yang, X., Mo, H. J., Li, C., & Jing, Y. P. 2005, *MNRAS*, 361, 1203
- Vanderriest, C., Schneider, J., Herpe, G., Chevreton, M., Moles, M., & Wlerick, G. 1989, *A&A*, 215, 1
- Weymann, R. J., et al. 1980, *Nature*, 285, 641
- Wilman, D. J., Balogh, M. L., Bower, R. G., Mulchaey, J. S., Oemler, A., Carlberg, R. G., Morris, S. L., & Whitaker, R. J. 2005, *MNRAS*, 358, 71
- Winn, J. N., Hewitt, J. N., Patnaik, A. R., Schechter, P. L., Schommer, R. A., López, S., Maza, J., & Wachter, S. 2001, *AJ*, 121, 1223
- Winn, J. N., Hall, P. B., & Schechter, P. L. 2003, *ApJ*, 597, 672
- Wisotzki, L., Koehler, T., Lopez, S., & Reimers, D. 1996, *A&A*, 315, L405
- Wyithe, J. S. B., Webster, R. L., Turner, E. L., & Mortlock, D. J. 2000, *MNRAS*, 315, 62
- Yonehara, A. 2001, *ApJ*, 548, L127
- Young, P., Gunn, J. E., Oke, J. B., Westphal, J. A., & Kristian, J. 1981, *ApJ*, 244, 736
- Zabludoff, A. I., Huchra, J. P., & Geller, M. J. 1990, *ApJS*, 74, 1
- Zabludoff, A. I., & Mulchaey, J. S. 1998, *ApJ*, 496, 39
- Zabludoff, A. I., & Mulchaey, J. S. 2000, *ApJ*, 539, 136